3 Results

3.1 Material tests

To find a suitable material for the µPCR chip, several materials were primarily investigated. The following figure shows a gelelectrophoretic endpoint analysis of a set of 10µl PCR tests (see 2.3.1) for different materials.

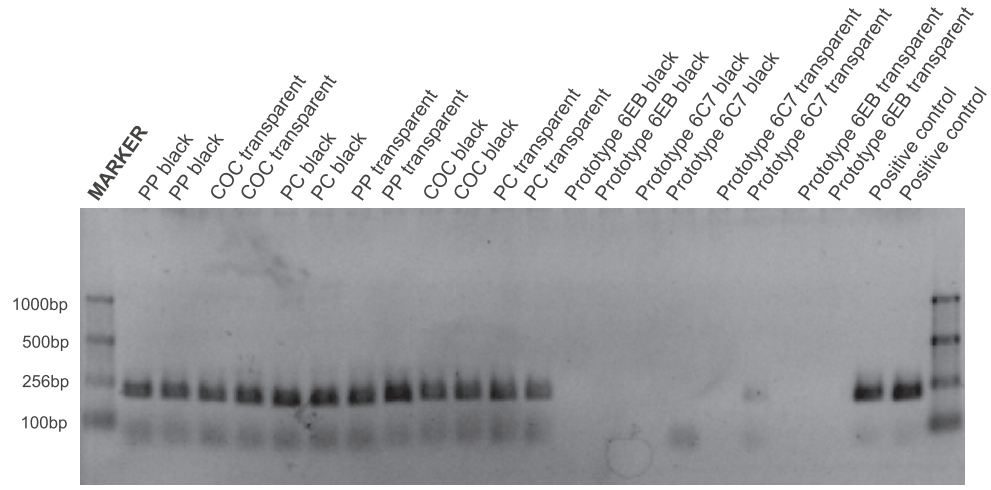

Figure 15: Gelelectrophoretic analysis of PCR material tests. PP, COC and PC samples show comparable enzyme activities for black and transparent. In all of these samples dimerisation is slightly higher, than in the positive control. This might be due to a changed thermo control because of the added material splitters. All prototypes for the lithographic fabrication show almost total inhibition of enzymatic activity.

Enzymatic activity, yield of the expected PCR fragment and the degree of dimerisation were evaluated. In Table 8 the results are summarized for all materials tested, including the results of the tests for thermo stability and background fluorescence. The investigated parameters were classified as follows: enzymatic activity (none, poor, medium, high), expected fragment (none, faint, normal), dimerisation product (none, faint, medium, strong), thermo stability (high, low) and fluorescence (lowermost, low, medium, high). The materials chosen for injection molding were all suitable with respect to their 'PCR compatibility'. Only transparent PP had to be excluded due to medium fluorescence intensity. Although photolithographic fabrication of microstructured devices is a promising approach, no photo-polymerisable material sample showed sufficient PCR compatibility. All covering materials had appropriate optical and thermal properties. Effects on PCR were mainly rendered by the used glue. Only AB–0558 showed swelling during the material test, caused by the direct contact to the reaction liquid.

Table 8: Summarization of results for all material tests

Material	Enzymatic activity	Yield of expected fragment	Degree of dimerisation	Thermo stability	Fluorescence
Materials for injection molding					
PP transparent	*high*	*normal*	*low*	*high*	*medium*
PP black	*high*	*normal*	*low*	*high*	*low*
COC transparent	*high*	*normal*	*low*	*high*	*lowermost*
COC black	*high*	*faint - normal*	*high*	*high*	*lowermost*
PC black	*high*	*normal*	-	-	-
PC transparent	*high*	*normal*	-	-	-
Materials for photolithographic fabrication					
Prototype 6C8	*none*	*none*	-	-	-
Prototype 6C7 black	*none*	*none*	-	-	-
Prototype 6C7 transparent	*none*	*none*	-	-	-
Prototype 6A9	*none*	*none*	-	-	-
Prototype 6C8	*none*	*none*	-	-	-
Prototype 6EB black	*none*	*none*	-	-	-
Prototype 6EB transparent	*none*	*none*	-	-	-
Prototype 77D	*poor*	*none*	*faint*	-	-
Prototype 1B06B/744	*none*	*none*	-	-	-
Materials for adhesive covering					
Optical Adhesive Covers (ABI)	*high*	*faint*	*medium*	*high*	*lowermost*
VIEWseal (Greiner)	*high*	*none*	*strong*	*high*	*lowermost*
AB-0558 (Ab-Gene)	-	*none*	-	-	*high*
Soft Sealing (MG Research)	*medium*	*faint*	*medium*	*low (plastic)*	*low*

Finally two potential chip materials fulfilled our requirements: PP black and COC. Due to COC's non-resistance against highly non-polar organic solvents such as mineral oil, black PP was finally chosen. From the tested sealing materials we opted for Optical Adhesive Covers from ABI for further experiments.

3.2 Liquid handling

Liquid handling is a crucial issue in miniaturization. Several advanced nanodispensing technologies were evaluated, used and adapted. At first, reliability of dispensing and the

impact of mixing were investigated. Two possible procedures were tested, to improve the dispensing reliability and to stabilize the nozzle performance: ultrasonic treatment of samples comprising large nucleic acids such as genomic DNA, which increase the sample viscosity and oil pre-aspiration for introducing a separation layer between sample and system fluid.

3.2.1 Dispensing accuracy of the piezo nanodispenser

The SciflexArrayer (Scienion) was operated in single nozzle mode (2.6.1). Aqueous solutions of a FAM dye labeled oligonucleotide (2.1) were aspirated in several concentrations to test the dispensing accuracy. Aliquots (8 replicates) of 200 nl, 150 nl or 100 nl were dispensed into the µPCR chip and quantified by fluorescence measurements (2.6.5). A comprehensive summary of intensities can be found in the appendix Table 15. For the 200 nl volumes the lower concentrated solutions (0.1 – 0.25 µM) showed, compared to the higher concentrated dye solutions (0.3 – 0.5 µM), an increased variation of CV values between 5.5% and 6.8%. Although less distinctly this is also apparent in the 150 nl and 100 nl dispenses with CV values ranging from 2.5% to 4.2% and 3.4% to 4.1%, respectively. The variation of higher concentrated dye solutions ranges between 1.5% and 3.7% for all three volumes. This increase in variation for the lower concentrated solutions could be caused by a stronger impact of adhesive effects between oligonucleotides or dye and the inner nozzle surface, since the ratio between molecules and surface is smaller. For evaluation of the dispensing accuracy higher concentrated solutions (0.3 – 0.5 M) show a good accuracy and reproducibility doing 8 dispenses of 200 nl, 150 nl and 100 nl volumes with mean CV values of 1.9%, 1.9 % and 3.0%, respectively. Although samples and system liquid are aqueous solutions, no distinct mixing could be detected by reduced fluorescence intensities for the late dispenses. The SciFlexArrayer was only used for dispensing of aqueous solutions with moderate concentrations of DNA, cDNA or oligonucleotides. Higher concentrated solutions as well as detergents containing reaction mixes (SybrGreen qPCR mix, TaqMan qPCR mix) frequently destroyed the nozzle performance and made both, reproducible and robust dispensing impossible.

3.2.2 Dispensing accuracy of the valve nanodispensers

Two nanodispensers were used, which are based on the valve dispensing technology (Seyonic). First tests for the accuracy of this dispensing technology were made with the custom-made valve dispenser (2.6.2). After aspiration of 7 µl of an aqueous tartrazine dye solution, 200 nl volumes were sequentially dispensed. Dispensed volumes were quantified (see 2.6.5). Although successive decreasing signal intensities, the inter nozzle variation for 4 nozzles remains stable, represented by the respective error bars and an averaged CV value of 3.6% per dispense. The overall CV value of 6.0% for all 16

dispenses reflects more the decrease of intensity, than a lack of reproducibility of the dispensed volumes. This is caused by dilution of the aspirated dye through mixing with system fluid. Since system fluid of the used nanodispensers is water, and samples as well as reaction mixtures are aqueous solutions, no separating barrier exists between both liquids. Mixing of sample/mix and system fluid starts in the nozzle immediately after aspiration. To compensate potential concentration changes due to mixing, always more material than needed was aspirated (see dispensing protocols 2.6.4). To better rate the reproducibility of dispensed volumes, only few dispenses per individual nozzle were taken for evaluation of variability. 3, 4 or 5 successively performed 200 nl dispenses resulted in averaged CV values of 1.8%, 2.1% and 2.4%, respectively, as an estimate of the nozzle dispensing reproducibility. Further experiments showed dependence between

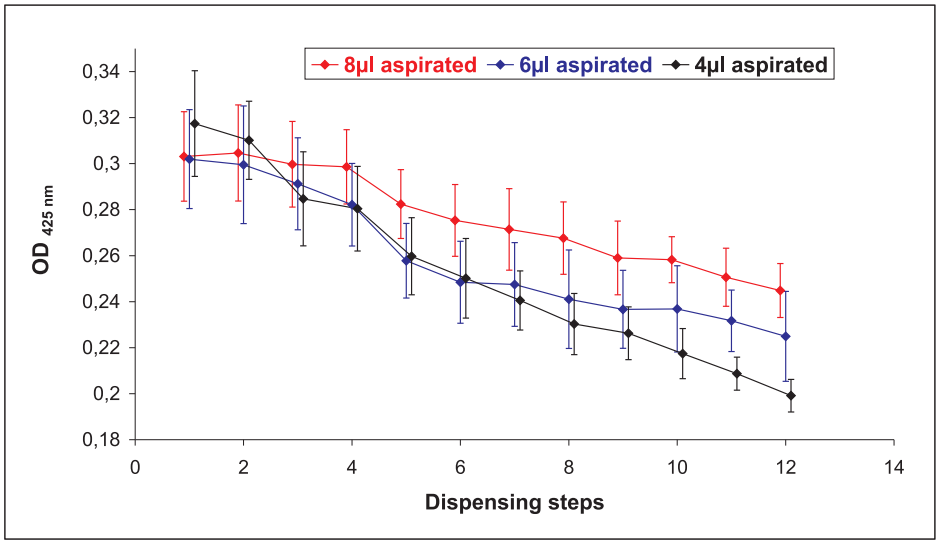

(a) Mixing effect for 3 different aspiration volumes

Figure 16: Mixing effects with the valve nanodispensing technology. After aspiration of different volumes of a tartrazine solution (5 g/l) each nozzle dispensed 12 times, 200nl each. Each curve represents the averaged dye intensity values for 8 nozzles.

aspirated volume and the degree of mixing. Figure 16 shows the progress of mixing during the dispensing process, and the degree of mixing during the first dispenses, which is inversively correlated with the aspirated volume. After aspiration of 4 µl, 6 µl or 8 µl of a 5 g/l tartrazine solution, 200 nl aliquotes were dispensed. Amounts of aspirated dye material were measured (see 2.6.5). For 4 µl and 6 µl aspirates immediately after the first dispense mixing is shown by a reduction of dispensed tartrazine. Only for the highest sample volume of 8 µl, the tartrazine concentration in the nozzle remains almost stable over the first 4 dispenses. This shows, that mixing is not only a local effect, but is easily transferred from the system liquid/sample solution border to the tip of the nozzle, even over an aspirated sample volume of 6 µl. Thereby it has almost with the first dispense impact on concentration of dispensed components such as target molecules.

3.2.3 Elimination of mixing effects by an oil separation layer

Reproducible dispensing of components could be considerably improved by introducing a lipophilic separation layer through pre-aspiration of polydimethylsiloxane oil. This was only possible with the valve dispensing systems (see 2.6.3). Figure 17 shows the different characteristic of mixing with and without oil pre-aspiration. In both cases 1 µl of an aqueous tartrazine solution (20 g/l) was aspirated. In case of oil separation 1 µl oil was aspirated in advance. After aspiration 100 nl aliquots were dispensed 24 times and amounts of dispensed dye were quantified (see 2.6.5). Both curves in Figure 17 represent averaged values of 8 nozzles. The dispensing procedure without separation

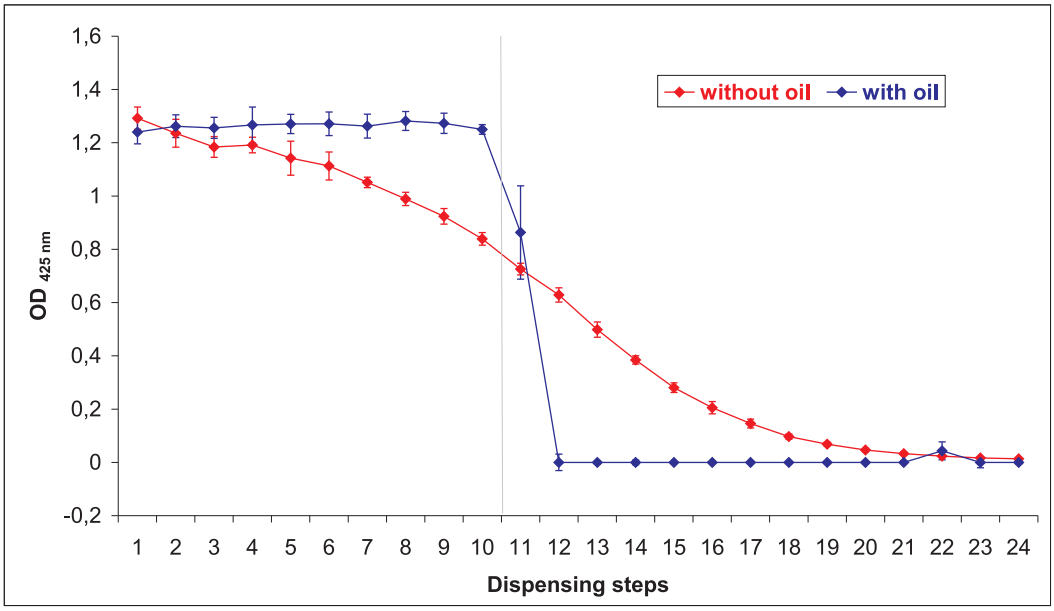

Figure 17: Efficiency of oil separation for the valve dispenser. One microliter of an aqueous tatrazine solution (20g/l) was aspirated and dispensed 24 times in 100 nl aliquots. In case of oil separation 1 µl oil was aspirated in advance. Both curves represent averaged values from 8 nozzles.

layer shows again a constant reduction of dispensed tartrazine caused by mixing. In contrast the dispensing procedure with oil pre-aspiration shows an efficient separation of system fluid and sample by equally distributed amounts of tartrazine for the first 10 dispenses. During the first 10 dispenses the inter nozzle variation (8 nozzles) is comparable between both dispensing procedures. The CV values are in average 3.1% for the 'with oil' procedure and 3.4% for the 'without oil' procedure. The oil separation layer significantly improves the reproducibility of dispenses with each individual nozzle and reduces the CV value for the first 10 dispenses to averaged 2.5%. At the 11^{th} dispense the signal breaks down, but still has some intensity. This can be caused by a higher aspiration volume than the sum of volumes dispensed. Starting from the 12^{th} dispensing step no tartrazine can be detected anymore. A signal increase at the 22nd dispense can be caused by a cleaning effect of the system fluid. Oil is covering the inner

Table 9: Comparison of performance parameters for fragmented and native human genomic DNA using the FlexArrayer (piezo). Only adjustments of voltage, which changes the final dispensing volume, helped to abide nozzle performance.

	pure hgDNA	**sheared hgDNA**
first concentration 5ng/l		
visual droplet check	perfect droplet	perfect droplet
dispensing quality on membrane	regular pattern, no missings	regular shape, no missings
voltage	104 V	104 V
second concentration 20 ng/l		
visual droplet check	perfect droplet only with increased voltage	perfect droplet
dispensing quality on membrane	regular pattern, no missings	regular pattern, no missings
voltage	**130 V**	104 V

nozzle surface and needs some washing time to be fully removed. This can be tracked during the last dispenses, which wash oil residuals and finally remaining tartrazine molecules from the surface.

Attempts to introduce an oil separation layer with the SciFlexarrayer were not successful. The nozzle performance became totally inconsistent after aspiration of polydimethylsiloxane oil due to partial or full loss of nozzle functionality.

3.2.4 Fragmentation of DNA for improved dispenser performance

Since the piezo dispenser more frequently showed a loss of nozzle performance with higher concentrated samples of hgDNA, than for samples of single stranded DNA and short fragments, a possibly correlation between fragment length and stable nozzle performance was investigated. Human genomic DNA in an aqueous solution with a concentration of 20 ng/µl was applied to ultrasonic treatment for 10 sec, 20 sec, 30 sec, 40 sec and 50 sec. The degree of fragmentation was checked by gelelectrophoretic analysis. At the shortest exposure time of 10 sec fragmentation ranged from approx. 500 to 5000 bp. The fragment size on average as well as the size range is decreasing by extending the exposure time. It ranges from 350 to 4000 bp, 350 to 3000 bp and 300 to 2000 bp length for exposure times of 20 sec, 30 sec and 40 sec, respectively. At an exposure time of 50 sec no fragments with a length above 2000 bp were detectable.

For investigation of nozzle performance two aqueous 20 ng/µl hgDNA solutions were prepared. One DNA solution was ultrasonically treated for 30 sec to fragment the DNA. Fragmented and non-treated DNA were compared with regard to their impact on nozzle performance using final DNA concentrations of 20 ng/µl and 5 ng/µl. For visualization of dispensed volumes on a white nitrocellulose membrane cresole red was added in a final concentration of 1 mM. After aspiration of 10 µl, 200 nl aliquots (48 replicates) were dispensed on the membrane. Table 9 summarizes the results for the comparison

of performance parameters. The droplet shape was visually evaluated, consistency of dispensing was checked on the membrane. Human genomic DNA in a concentration of 20 ng/µl highly affects the nozzle performance of the piezo dispenser. According to the higher concentration voltage had to be manually adjusted, which causes a change in the dispensed volumes. This intervention complicated the process of dispensing and made it vulnerable to handling errors. Fragmentation of the genomic DNA could be shown to circumvent this. No adjustment of any parameter was necessary.

Native and ultrasonic treated (30 sec and 50 sec) hgDNA was used in a concentration gradient experiment to investigate the effect of fragmentation on PCR efficiency. A 10 µl SybrGreen assay for NOD2_SNP8 was performed with a gradient of 6000, 600 and 60 initial target molecules. As shown in Figure 18 the fragmentation caused reduced Ct-values. The shift is consistent over all concentrations, which indicates no impact on the PCR efficiency, but on the sensitivity of the method. Calculation of PCR efficiency results in 114%, 99% and 119% for the non-treated, 30 sec and 50 sec sample, respectively. To stabilize the dispensing performance, fragmentation of sample DNA is an option, but this also means a reduced sensitivity of the method, which can be disadvantageous for low concentrated targets.

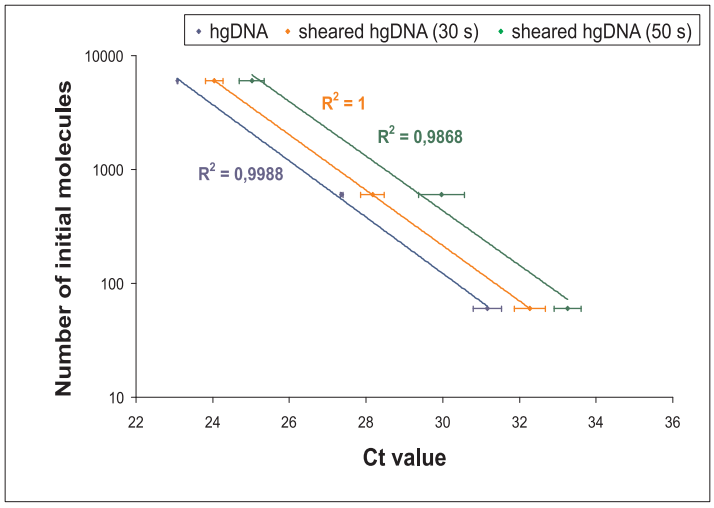

Figure 18: Impact of DNA fragmentation on PCR efficiency. Triplicates of SybrGreen assays with three different hgDNA concentrations were performed in 10 µl. Ultrasonically treated samples show a shift (delay) in absolute Ct-values, indicating a reduced sensitivity.

3.3 A workflow suitable for the nanoliter-scale

For miniaturized systems the workflow is not only determined by the number and requirements of each working step, but also by miniaturization specific issues such as evaporation. The µPCR chips were filled in a four-step procedure including preloading of sample DNA, desiccation of samples (see 2.9.5), distribution of the reaction mix and immediate sealing. Desiccation of samples eliminates a possible impact of

evaporation after sample pre-loading on the final volume. Evaporation is a crucial issue for miniaturized systems, as small volume fluctuations notably alter signal intensities. This four step procedure limits variation in end volumes to the mix dispensing step and occurring evaporation between mix dispensing and sealing. Separation of sample dispensing and dispensing of target specific reaction mix enables more flexibility in the configuration of the µPCR chip. Furthermore this procedure lowers the risk of cross contaminations. After mix dispensing the µPCR chip is immediately sealed. To ensure tight sealing pressure is manually applied from top with a flat surfaced metal block. The sealed chip is centrifuged at 2000 rpm for 1 minute, placed in the cycler and processed. This is followed by image analysis and data analysis.

3.3.1 Desiccation had no significant effect on the quantification result

To investigate a possible effect of the DNA desiccation on PCR performance, dried versus aqueous DNA samples were compared in 10 µl standard TaqMan assays (see 2.2.3) on a concentration gradient of human genomic DNA (Figure 19).

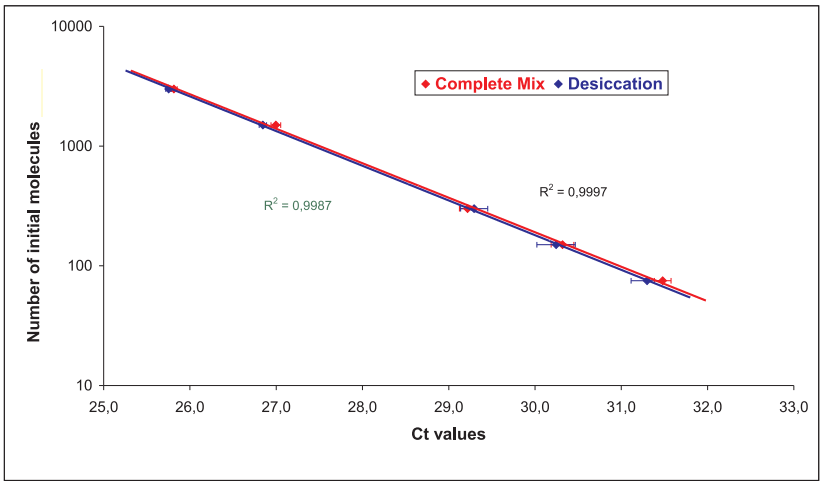

Figure 19: Comparison of real-time PCR performance for desiccated samples vs. completely dispensed assays. Standard TaqMan assays for RNAseP were performed on a gradient of 3000, 1500, 300, 150 and 75 initial molecules human genomic DNA.

Amplification of the RNAse P TaqMan assay showed no significant differences between desiccated and non-desiccated samples. The resulting standard curves have a similar correlation coefficient of 0.99. The amplification efficiencies on the aqueous and dried samples were not significantly changed with 94.1% and 94.8%, respectively. Consequently the desiccation step does not affect the results of a real-time PCR based analysis with the TaqMan technology.

3.3.2 Surface adsorption effects on PCR performance

Surfaces tend to be charged, which also applies to polymers and results in interactions between reactants and surface. To test for the effect of a positively vs. negatively

charged surface µPCR chips were functionalized with AAM for amino functionality and GMC for epoxy functionality (see 2.5). 200 nl Standard TaqMan assays targeting RNAse P were performed in treated and untreated chips. Template was the RNAse P assay flanking PCR product (2.9.1) with following initial target molecule numbers per 200 nl reaction: 4.3×10^5, 4.3×10^4, 4.3×10^3 and 4.3×10^1. The AAM treated chip

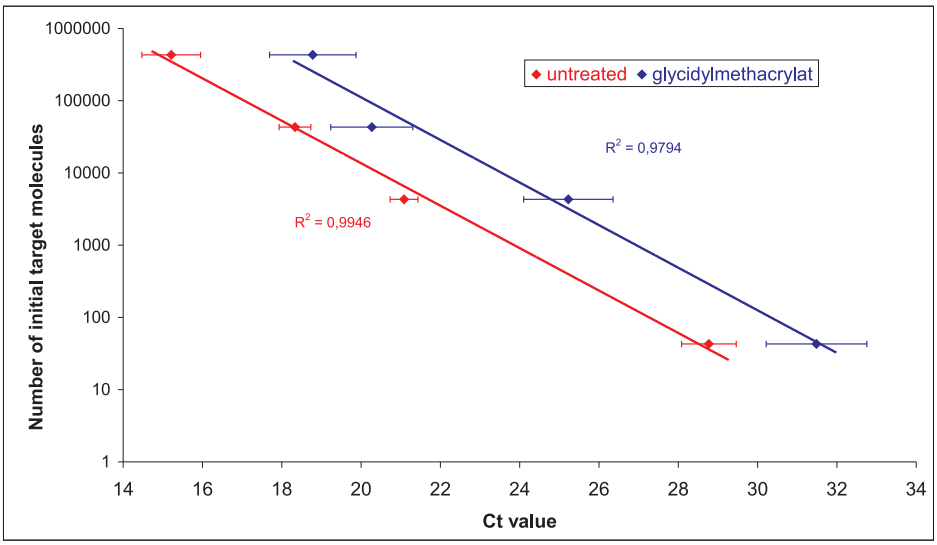

Figure 20: Comparison of real-time PCR performance between non-treated and a GMA-treated chip. The GMA chip with epoxy functionality shows reduced Ct-values for all concentrations. Shift is consistent over all concentrations, which means that the PCR efficiency is comparable to the non-treated µPCR chip.

showed no successful amplification. Although no PCR inhibitory effects of this substance are known in literature, I assume other reasons than an adhesion caused inhibition of the PCR. As shown in Figure 20 the µPCR chip with epoxy functionality shows increased Ct-values with an average offset of 1.5 cycles between non-functionalized and functionalized surface. Standard deviations range between 0.35 and 0.74 cycles for the non-treated and between 1.03 and 1.27 for the epoxy chip, indicating a much higher variation for the modified chip. However, comparable PCR efficiencies for treated and non-treated chip of 97.2 % and 96.7% respectively, do not show a significant change of PCR performance. Only a decreased sensitivity of the epoxy functionalized PCR chip was found, probably caused by adhesion induced reduction of available target molecules or enzyme molecules. The detected number of initial molecules differs in one to two orders of magnitude ($\Delta Ct = 1.5$) between both chips.

3.4 Feasibility of PCR in nanoliter range

3.4.1 Endpoint measurements

To investigate the feasibility of PCR in nanoliter volumes, first tests were made in flat shaped MicroAmp Caps (Applied Biosystems). The flat inner surface of the cap was

slightly drilled to produce cavities with a volume of approximately 150 – 250 nl. Cavities were used to localize the dispensed volumes, which were covered with a layer of mineral oil. A standard PCR using the Mu5 primers and a final template concentration of 1 ng/µl hgDNA was performed in 180 nl, 90 nl, 45 nl and 18 nl (see 2.2.1). In Figure 21 PCRs are shown after staining by adding the same volume as the reaction volume of a 20 × aqueous SybrGreen solution. Increased fluorescence intensities were

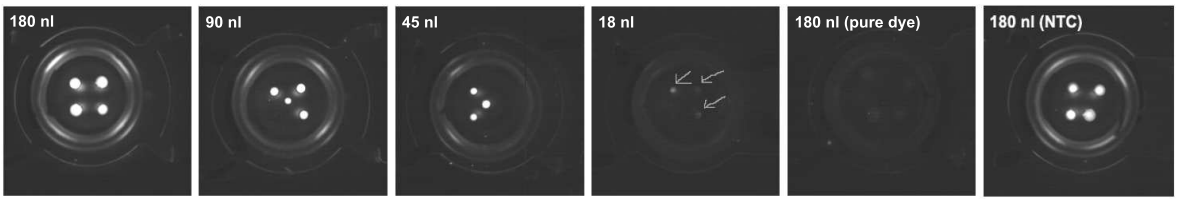

Figure 21: Endpoint quantification of PCR product with an intercalating dye (SybrGreen) for 180 nl, 90 nl, 45 nl and 18 nl reactions.

observed for all volumes. Reactions of 90 nl and below showed moving droplets during the PCR. Small (and light) droplets were displaced upwards by mineral oil that slid between the aqueous droplet and the reaction vessel surface. The non-template control for the 180 nl volume showed a low but still distinctive signal intensity. A single endpoint measurement of a PCR reaction stained with intercalating dyes does not allow to differentiate between PCR product and potential primer dimerization artifacts. Due to the low volumes and the relatively high amount of mineral oil no gelelectrophoretic analysis could be performed to examine the degree of possible dimerization, but results indicate successful amplification down to 18 nl volumes.

Miniaturized PCR without oil

To allow gelelectrophoretic verification of the expected PCR product a miniaturized standard SybrGreen assay (see 2.2.2) with the NOD2_SNP8 primer set (see Table 1) was performed without oil sealing. Instead of the caps a black colored COC based 3456 well plate (Greiner) was sealed with a polypropylene based adhesive sealing foil (Greiner). SybrGreen assays (Qiagen) were performed in 1 µl, 500 nl and 200 nl. Final template concentrations of human genomic DNA in 1 µl volumes were 1.5 ng/µl (450 molecules), 0.5 ng/µl (150 molecules), 0.1 ng/µl (30 molecules) and 0.05 ng/µl (15 molecules). For 500 nl and 200 nl PCRs the template concentration was 1.5 ng/µl. The plate was processed in the real-time hydro cycler unit (see 2.7.3), which enabled to monitor the fluorescence in real-time from top. An endpoint measurement of intensities was done at room temperature. For 1 µl volumes endpoint fluorescence measurements showed slightly lower (11306 ± 1794) intensities than for positive controls (12071 ± 970). 500 nl assays even showed a 7% higher fluorescence intensity for non-template reactions than for DNA containing PCRs. To test for potential contamination, PCRs were pooled and electrophoretically analysed (Figure 22). In the gel analysis PCRs of all volumes showed

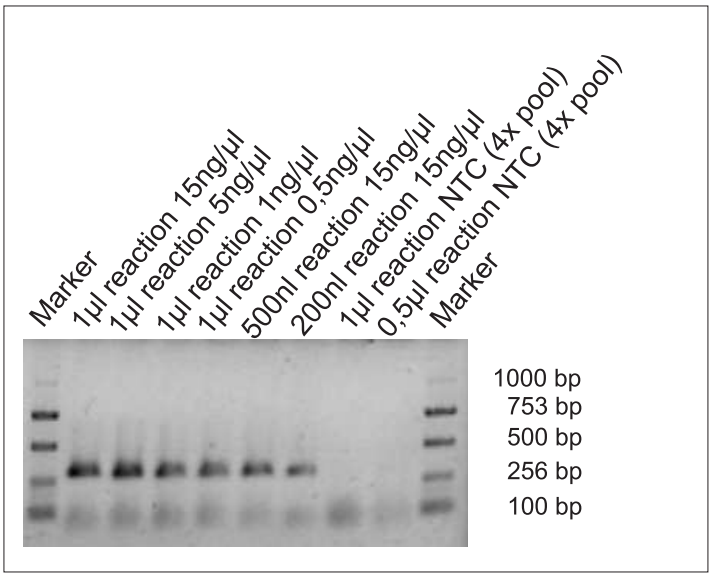

Figure 22: Gelelectrophoretic analysis of pooled 1 µl, 500 nl and 200 nl reactions. Before loading on the gel reactions were pooled to allow better visualisation. The number of pooled reactions per lane are stated in brackets. All reactions show the expected PCR product but also dimerisation products.

the expected PCR fragment as well as products of primer dimerisation. The amount of primer dimerisation artifacts seems to be increased for the non-template controls and explains the high signal intensities of endpoint measurements of non-template controls. This does not necessarily have to cause problems for applications following the PCR amplification step, but complicates the control for successful amplification by a single fluorescence measurement using intercalating dyes. Successful amplification without use of oil sealing could be verified down to an reaction volume of 200 nl.

3.4.2 Real-time monitoring of amplification

In contrast to endpoint measurements real-time fluorescence monitoring provides more information about PCR performance. This enables to directly monitor the amplification of the intended fragment. Real-time analysis of the performed miniaturized PCRs shows a high impact of the observed primer-dimer artifacts (see Figure 22) on resulting fluorescence measurements (Figure 23).

The amplification plot of the non-template control shows a late but distinct rise in fluorescence due to the formation of primer-dimerisation products. Resulting Ct-values are close to the values of the low concentrated targets. This could be misleading in the interpretation of the real-time quantification results. Primer dimerisation products that contribute to the measured fluorescence in PCRs with non-template or low concentrated template lead to a measurable Ct-value or a lower Ct-value, respectively. This causes an overestimation of the determined amount of initial template.

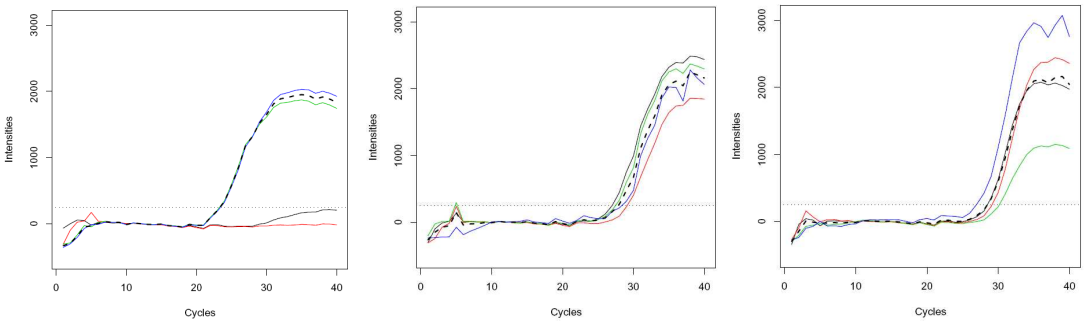

(a) 1.5 ng/µl hgDNA **(b)** 0.1 ng/µl hgDNA **(c)** non-template control

Figure 23: Realtime analysis of SybrGreen assays in 1 µl, performed in the COC-based 3456-well plate (Greiner). **a)** Initial target concentration of 1.5 ng/µl human genomic DNA (app. 450 molecules), mean Ct-value 23.4±0.10 **b)** Initial target concentration of 0.1 ng/µl human genomic DNA (app. 30 molecules), mean Ct-value 28.0±0.94 **c)** non template control, the dotted line marks the average of the performed reactions, mean Ct-value 28.7±1.35.

3.4.3 Intercalating dye vs. probe based chemistry

The so clearly observed impact of primer dimerisation in the 1µl volume and below raised the question, whether this applies especially strong to low volumes. Standard SybrGreen assays (ABI) in several volumes and the RNAse P primer set were performed in the ABI Prism 7900 HT (see 2.2.2). Since the probe based approach avoids false-positive results due to primer dimerisation TaqMan assays (see 2.2.3) were performed for comparison. Each reaction was done in triplicates. Assay volumes were 10 µl, 8 µl, 5 µl, 3 µl, 1.5 µl and 500 nl. Template was the RNAse P TaqMan flanking PCR product (see 2.9.1) with following concentrations: 2.2×10^6 molecules/µl, 2.2×10^5 molecules/µl, 2.2×10^4 molecules/µl, 2.2×10^3 molecules/µl and 2.2×10^2 molecules/µl.
Although a drastic reduction of the SybrGreen assay volume no formation of primer dimers in template containing reactions could be observed by melting curve analysis. Only the non-template controls showed dimerisation which results in a Ct-value of 31.9 ± 1.2. In the parallel TaqMan experiment no amplification was detectable for non-template controls.

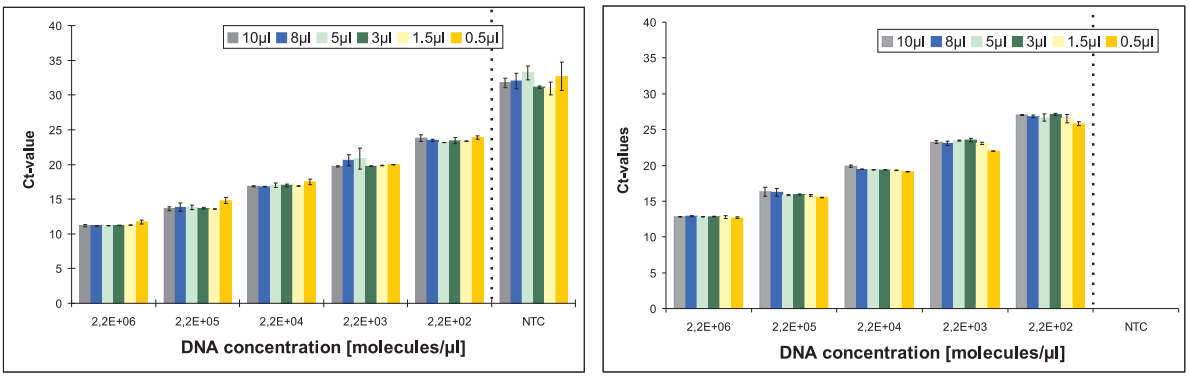

(a) SybrGreen **(b)** TaqMan

Figure 24: Comparison of effects by primer dimerisation on Ct-values for small volume PCRs with SybrGreen and TaqMan in a 384 well standard format **a)** Standard SybrGreen assays of several target concentrations in 10 µl, 8 µl, 5 µl, 3 µl, 1.5 µl and 500 nl. Non-template controls (NTC) show late Ct-values due to dimersiation artifacts. **b)** Standard TaqMan assays with the same target concentrations and volumes. NTCs show no Ct-values since no dimerisation artifacts were detected by the probe based approach.

Interestingly even the Ct-values of PCRs with the same DNA concentration showed no significant changes between different volumes, which also applies to the calculated efficiencies for all SybrGreen and TaqMan assays in Table 10.

Table 10: Comparison of assay efficiencies between SybrGreen and TaqMan assays

	10 µl	**8 µl**	**5 µl**	**3 µl**	**1.5 µl**	**0.5 µl**
SybrGreen						
R_2	0,993	0,997	0,995	0,996	0,996	0,995
Efficiency	107,7%	107,5%	109,1%	111,7%	112,3%	117,2%
TaqMan						
R_2	1,000	0,999	0,998	0,997	0,999	0,997
Efficiency	91,7%	93,9%	91,6%	89,0%	93,4%	101,8%

No systematic changes in efficiency with reduced assay volumes were observed; only the fluorescence data in the low volumes of 1.5 µl and 500 nl were quite noisy. This could be an instrument issue, but also concentration dependend, since this especially applied to the low target concentrations and non-template reactions. Finally the probe based approach (TaqMan) was chosen to study the feasibility of real-time PCR in the low nanoliter volume range. In respect to the application in a large scale setting it allows a more straight forward strategy for highly miniaturized PCR based applications.

3.5 Feasibility of real-time quantification with 200 nl TaqMan assays

3.5.1 Sensitivity of 200 nl TaqMan assays

Shrinking of a standard 10 µl reaction volume down to 200 nl results in a 50-fold reduction of initial molecules. Thus, the maximal detection sensitivity of the system was investigated using 200 nl RNAse P TaqMan assay, performed with 10, 5, 1, 0.5 and 0.2 initial human genomic DNA molecules in the µPCR chip (1k-format). DNA was preloaded with the piezo dispenser and desiccated as described above (2.9.5). The mix was dispensed with the custom-made valve dispensing station following the standard dispensing protocol (2.6.4). Successful amplification was determined by endpoint mea-

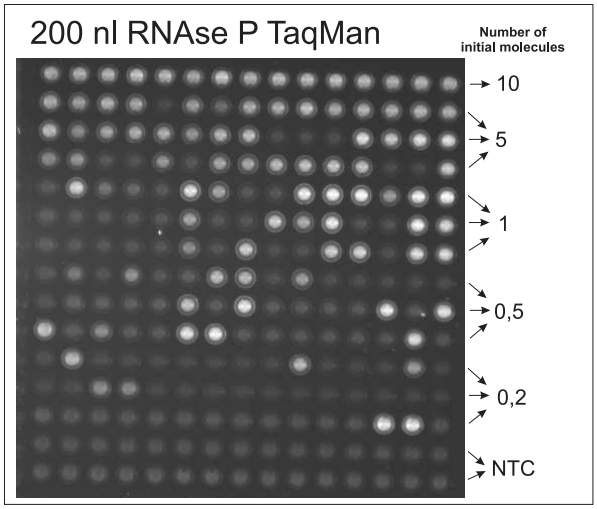

Figure 25: First concentration Gradient experiment with RNAseP in 200 nl

surements of fluorescence and scored (see 2.10.2). Reactions with 10 initial molecules were all positive for 45 replicates. Lowering the number of initial DNA molecules to 5, 1, 0.5 and 0.2 lead to a decrease of positives down to 78%, 53%, 44% and 16%, respectively (details see Table 11). The fact that for a theoretical or better statistical distribution of 0.2 initial molecules still one of five reactions are positive denotes a high sensitivity of the system. Nonetheless, the percentage of positives with 1 and 0.5 initial molecules do not reflect the expected trend. Possible reasons could be the varying distribution of target molecules per dispense, which especially applies to low concentrated samples, mixing effects between sample and dispenser system liquid, and the stronger influence of adhesive effects for lower numbers of molecules seen with the piezo dispenser (3.2.1).

Addressing the mixing as well as sensitivity issue, a further experiment in the µPCR chip (1k-format) was done with lowest numbers of initial target molecules. RNAse P TaqMan assays were performed in 200 nl with initial 10, 5, 2, 1, 0.5 and 0.2 target molecules. To avoid possibly mixing of system liquid and sample solution, the Sciclone valve dispensing unit was used with the newly developed *Oil separation*

dispensing protocol (2.6.4), to dispense DNA and mix.

Table 11: Sensitivity – 200 nl PCR with low numbers of initial molecules

	Standard dispensing protocol		*Oil separation dispensing protocol*	
Number of initial target molecules	**performed**	**successful**	**performed**	**successful**
10	45	100%	232	99,6%
5	45	77,8%	232	98,7%
2	–	–	406	92,0%
1	45	53,3%	832	73,9%
0.5	371	43,9%	832	48,1%
0.2	45	15,6%	832	27,0%

The experiments with tartrazine (see 3.2.3) have already shown, how efficient mixing can be avoided by introducing the oil separation into the dispensing protocol. This seems to be confirmed by the low target molecule number experiment. Assays with 10 and 5 initial target molecules show corresponding percentages of successful amplifications. The reduction of initial target molecules down to 1 shows a lower percentage of successful reactions, which is caused by distribution effects.

3.5.2 Quantification capability with 200 nl TaqMan assays

To investigate the suitability of the platform for real-time quantification, RNAse P TaqMan assays were performed on human genomic DNA with 1, 5, 10, 50 and 100 starting molecules doing 60, 60, 30, 30 and 30 replicate reactions, respectively. All components

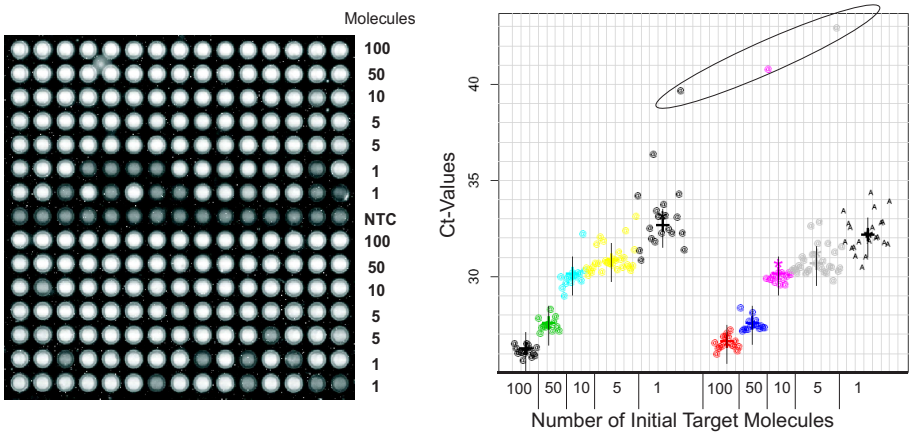

(a) Image of 1k-µPCR Chip at endpoint

(b) CT-value plot for 200 nl RNAse P Taqman assays

Figure 26: a) Shows the image taken of the chip in the 45^{th} cycle. In the right column the number of target molecules at the beginning are stated. **b)** Plot of all Ct-values for RNAse P TaqMan assays in 200m nl on hgDNA in several concentrations down to 1 initial target molecule per well.

were dispensed using the Staccato nanodispenser with oil separation. Concentrations were row wise arranged in two blocks as shown in Figure 26 a.

Reactions with initially 1 target molecule show 27% failing amplifications, which is concordant with the results from the sensitivity test. A plot of all Ct-values (Figure 26 b) clearly shows the relation between initial number of target molecules and variation. Three values are marked as being outliers, because they are more than 15% distanced to the median of all replicates (see outlier test 2.10.4). These values were excluded from further calculations. Absolute Ct-values, their standard variations and corresponding coefficients of variation (CV) can be found in Table 12. A plotted standard curve is shown in Figure 27 a.

For comparison to a conventional format a concentration gradient experiment was performed in 10 µl volumes on a standard platform (see 2.7). The initial numbers of target molecules were 4500, 3000, 1500, 300, 150 and 75 per reaction (duplicates); resulting mean Ct-values, corresponding standard deviations and CV values are shown in Table 12. The obtained Ct-values of the 10 µl assays show a much lower variation,

Table 12: Comparison of variation in absolute Ct-values between 200 nl and 10 µl volumes. Variation is represented by the standard deviation (SD) or respective coefficient of variation (CV). The last row shows an estimate of variation in percent molecules from the initial number.

target molecule numbers	**replicates**	**Ct-value$_{mean}$ ± SD**	**CV**	$\pm\%Molecules$
		200 nl assays		
100	30	26.4±0.38	1.4%	31%
50	30	27.5±0.33	1.2%	26%
10	60	30.0±0.51	1.7%	23%
5	60	30.9±0.71	2.3%	64%
1	60	32.6±1.27	3.9%	142%
		10 µl assays		
4500	2	25.8±0.06	0.2%	4%
3000	2	26.3±0.02	0.7%	1%
1500	2	27.6±0.06	0.2%	4%
300	2	30.0±0.11	0.4%	7%
150	2	31.1±0.07	0.2%	5%
75	2	32.1±0.04	0.1%	3%

than the 200 nl assays. This becomes especially apparent comparing reactions with few initial target molecules. The trend of increasing variation by decreasing target numbers was not observed in the 10 µl assays. Higher standard deviations of the mean Ct-values for 200 nl assays indicate a decreased reproducibility, especially for values > 30.Due to the exponential scale of the Ct-value, the impact of its variation can be difficult to access. Thus, standard deviations were used to estimate the variation in percent

molecules based on the following equation:[104]

$$\pm \%Molecules = [(E+1)^{SD} - 1] * 100\% \quad (3)$$

where SD is the standard deviation in Ct-values generated from replicate amplifications, E the efficiency of amplification, accessed via regression analysis of the constructed standard curves (Figure 27). For 200 nl assays an averaged efficiency of 100% was taken, to compensate the underestimation of Ct-values for the 1 target molecule assays. The plotted standard curves for both volume ranges (Figure 27) with correlation coefficients of 0.990 (200 nl) and 0.999 (10 µl) demonstrate a good accuracy for the reflection of a target concentration gradient by the obtained Ct-values, and therefore a good quantification capability of the miniaturized platform. In terms of amplification efficiency the

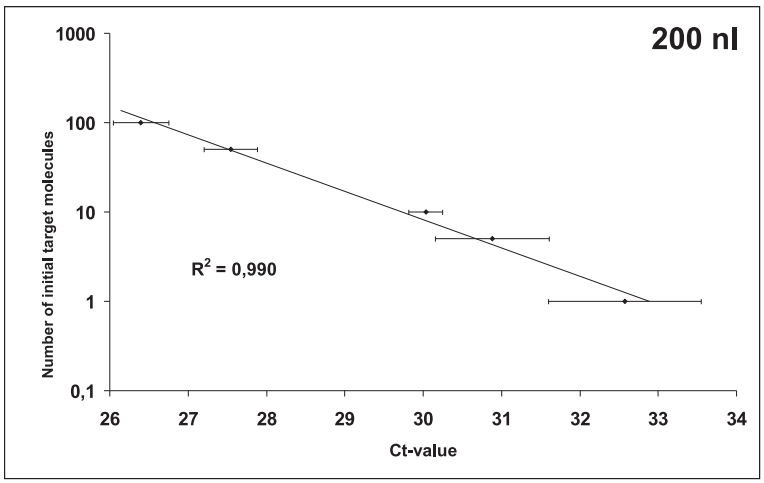

(a) Standard curve for 200 nl TaqMan assay – oil separation

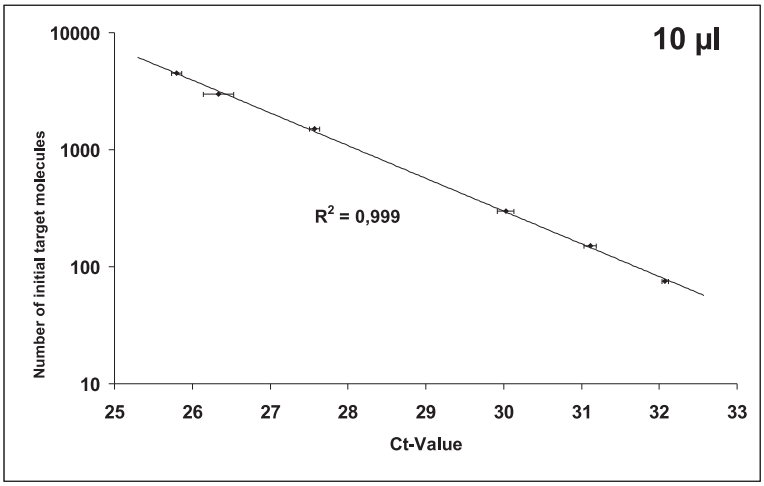

(b) Standard curve for 10 µl TaqMan assay

Figure 27: Comparison of variation between 10 /textmu l volumes and 200 nl volumes **a)** Standard curves for 200 nl assays with 100, 50, 10, 5 and 1 initial target molecules per well. **b)** Standard curve for 10 µl assays with initially 4500, 3000, 1500, 300, 150 and 75 target molecules

reactions in large volumes reached 90.5%, whereas at the nanoscale the efficiency was at 107%. The efficiency calculation is only estimation. Often varying values are shown in conventional as well as small volumes. So it is hardly to reason, whether this is a significant change in PCR efficiency. Results from experiments with higher numbers of initial target molecules (see 3.5.4), which were performed to evaluate the dynamic range of the µPCR chip platform, showed also efficiencies close to 100%. A failing rate of approx. 30% indicates, that the average number of target molecules per well must be higher, than nominal expected. Theoretically 1 molecule should be distributed per dispense into one well. Removing the values for the 1 molecule experiment reduces the 200 nl assay efficiency to 94% and increases the correlation coefficient to 0.998. This shows the effect of the Ct-value underestimation for the 1 molecule experiments on the efficiency calculation. A smaller average Ct-value for the 1-molecule assays leads to an increased slope of the standard curve, which causes an overestimation of the efficiency.

Final outcome of an expression profiling study is the fold change in expression. With the shown experiments fold changes between different concentrations can be calculated from the Ct-values and compared to the expected ratio, shown in Table 13. Expected and obtained fold changes showed comparable values for all 10 µl assays,

Table 13: Shown are fold changes for the the 200 nl and 10 µl experiment. Nominal fold changes were calculated from the numbers of initial target molecules. ΔCt-values are all > 0 because Ct-values of lower concentrated samples were subtracted from higher concentrated samples.

target molecule numbers	**nominal fold change**	**calculated ΔCt$\pm$SD**	**CV**	**calculated fold change**
		200 nl assays		
100 vs. 50	2	1.15±0.71	62%	2.2
50 vs. 10	5	2.49±0.84	34%	5.6
10 vs. 5	2	0.85±1.22	144%	1.8
5 vs. 1	5	1.69±1.98	117%	3.2
		10 µl assays		
4500 vs. 3000	1.5	0.53±0.26	49%	1.4
3000 vs. 1500	2	1.23±0.26	21%	2.3
1500 vs. 300	5	2.46±0.17	7%	5.5
300 vs. 150	2	1.09±0.18	17%	2.1
150 vs. 75	2	0.96±0.12	13%	2.0

and for the 200 nl assays with higher template concentrations. The fold change for 10 vs. 5 initial target molecules in 200 nl shows a slight underestimation, and the 5 vs. 1 molecule pair shows a significant underestimation. This is caused by the underestimated Ct-value for the low molecule assays as described above, which leads to a reduced difference between both Ct-values and therefore to a lower fold change.

3.5.3 Replicate number evaluation for 200 nl assays

Performing 15 or more replicates of an assay to obtain a sufficient result is surely impractical and inefficient. Therefore data of the experiment shown above was analyzed to investigate the explanatory power of smaller subgroups comprising 1 to 9 replicates. First of all the Ct-values for each concentration were investigated for their distribution (Figure 28). The box plots show a non-normal distribution. Due to the exponential

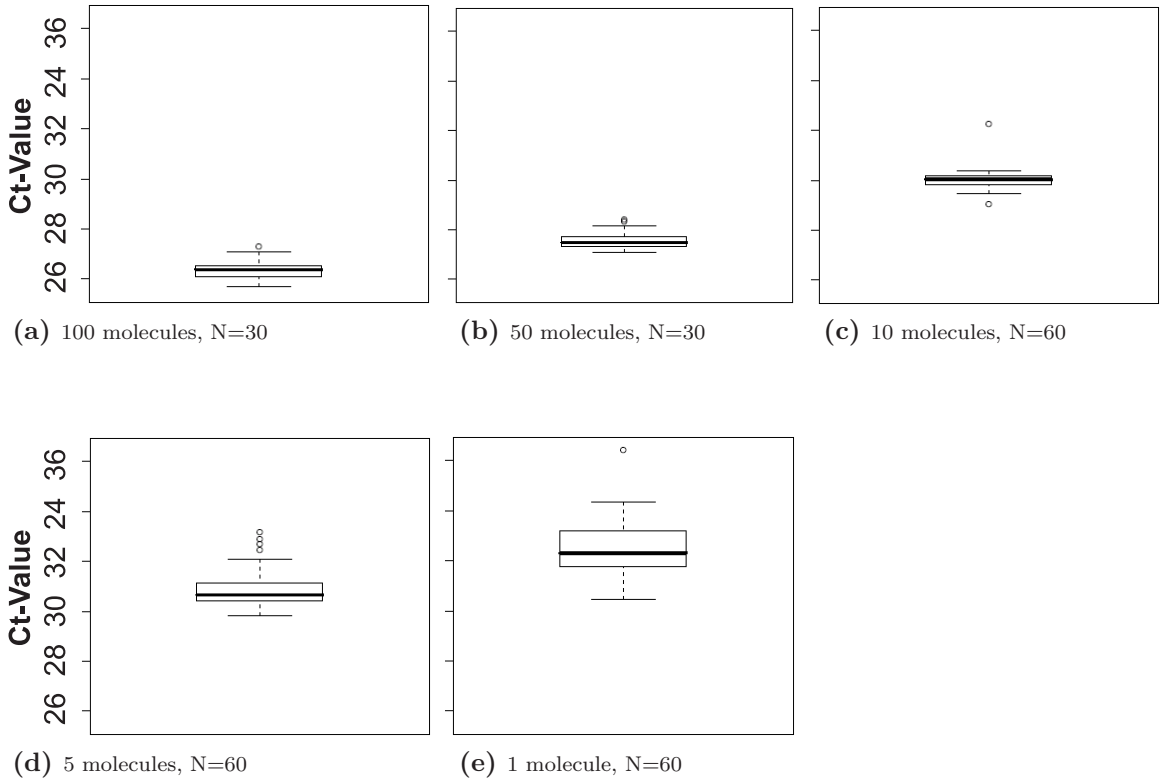

(a) 100 molecules, N=30 **(b)** 50 molecules, N=30 **(c)** 10 molecules, N=60

(d) 5 molecules, N=60 **(e)** 1 molecule, N=60

Figure 28: a – e) Visualization of Ct-value distribution with box-and-whisker diagrams (box plot) for all initial target concentrations.

nature of the PCR reaction the Ct-values, as a result of normally distributed target molecules during dispensing, are not expected to be normally distributed. This relation is described by the following equation:

$$N_t = N_0 * 2^{Ct} \tag{4}$$

N_t is the number of amplicons at the set threshold fluorescence, N_0 the number of initial target molecules and the Ct, the cycle at threshold. Because all reactions are compared at the same fluorescence intensity threshold, N_t is constant and thus the following relation between N_0 and the Ct-value persists:

$$N_0 \sim \frac{1}{2^{Ct}} \tag{5}$$

This can be used to transform the Ct-values with an exponential nature to a non-exponential form, which better reflects the distribution of initial target molecules as a source of variation for the Ct-values. The transformed values show only few extreme values in box plot analysis (not shown). For explanation, any transformed Ct-value which lies more then 1.5× the interquartile range (IQR) lower than the first quartile and 1.5× IQR higher than the third quartile is considered an extreme value. Another representation shall be used to show the effect of the transformation and to demonstrate the normal distribution of the data. The following Q-Q-Plots (Figure 29) show the comparison of a theoretical normal distribution and the sample distribution (100 initial molecules per well) by plotting both data against each other. In case of substantial deviations from a straight line no normal distribution of the samples is given. The plots

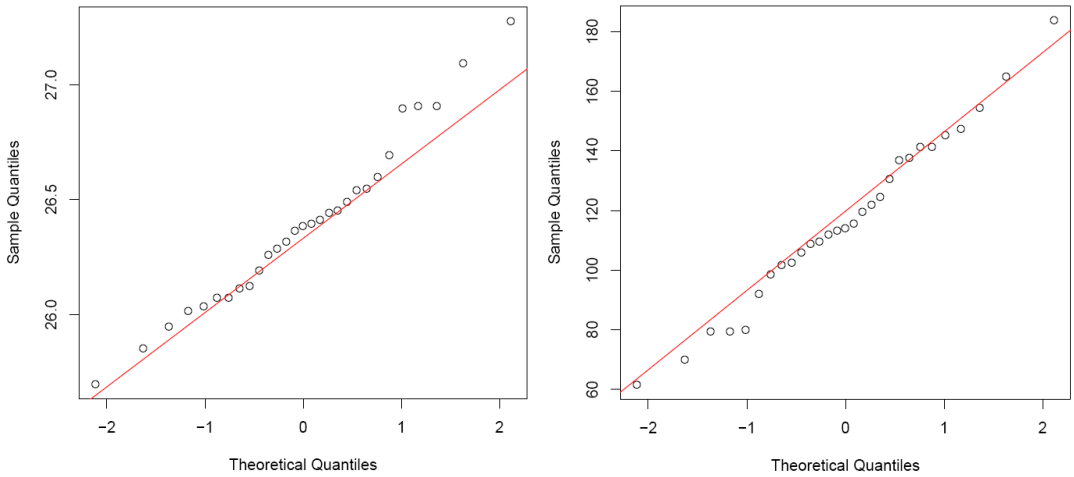

(a) Q-Q-Plot for raw Ct-values **(b)** Q-Q-Plot for transformed Ct-values

Figure 29: Comparison of Q-Q-Plots for raw and linearized Ct-values. **a)** Higher Ct-values seem to be out of the normal distribution trend (red line). **b)** Normalization respective linearization of raw values shows normal distribution of data.

demonstrate that the data set for 100 initial target molecules was normally distributed. This was tested for all five data sets. All were normal distributed and thus taken as an approximation of the *true value*. Only the 15% outlier rule (see 2.10.4) was used to remove outliers (3 values).

To access the possible variation in smaller subgroups of Ct-values from the original data set, mean Ct-values from randomly generated subgroups (N = 1 to 9) were calculated and compared to the complete data set (N = 30 and 60, respectively), which was the best approximation to the true value. Confidence intervals (CI) at a confidence level of 95% were calculated for the complete data sets of each template concentration (details see 2.10.7). This was done based on the transformed data, since the CI needs a normal distribution. Assuming a known standard deviation σ, we get the following

formulas for the right and left CI border:

$$\bar{x} - u_{1-\frac{\alpha}{2}} * \frac{\sigma}{\sqrt{n}} \quad ; \quad \bar{x} + u_{1-\frac{\alpha}{2}} * \frac{\sigma}{\sqrt{n}} \tag{6}$$

α means the probability and u the corresponding quartile of the normal distribution (p. 160, Hartung et al.[105]). In this example however the standard deviation must be guessed out of few values of samples. Therefore we used the t value instead of the u value, where s is the measured standard deviation.

$$\bar{x} - t_{n-1;1-\frac{p}{2}} * s * \frac{1}{\sqrt{n}} \quad ; \quad \bar{x} + t_{n-1;1-\frac{p}{2}} * s * \frac{1}{\sqrt{n}} \tag{7}$$

Since data sets for different numbers of initial target molecules had different sizes N, data sets were normalized to a fixed replicate number of $N = 60$ for better comparison using the following equation:

$$CI_{normalized} = (R - L) * \frac{\sqrt{n}}{\sqrt{m}} \tag{8}$$

$CI_{normalized}$ is the normalized interval width, L the original left interval edge, R the right one. The number of made replicates is n, m the new (normalization) total number of replicates, which is constant $N = 60$ over all target concentrations. Edges for $CI_{normalized}$ were calculated by addition and substraction of $CI_{normalized}/2$ to and from the mean, respectively. To simulate results with fewer replicates and compare these to the large data set, subsets of 1 – 9 replicates were randomly taken from the original data set. This was done 10.000 times to get a good representation of the variability in the original data. For each subset the mean and median were calculated and tested, if the obtained value lays within the normalized CI. The calculated (normalized) confidence interval shows a range, where the true value lays with a probability of 95%, based on a measurement with 60 replicates. In Figure 30 the percentages of results within the CI (N = 60) are shown. For both calculation methods the size N of a sub-sample correlates with the probability to lay inside of the CI, respective to be close to the true value. The mean from a subset is more susceptible to extreme values or outliers than the median. This is observed in the trajectories for the 10 molecule assays. The box-whisker-diagram (see Figure 28c) shows two extreme values, which have direct impact on the reliability of the resulting mean Ct-value of a subsample. Starting with 20 – 30% for a single measurement the reliability for a 9-fold measurement ranges between 40 and 75%, depending on the number of target molecules.

Although no plateau leveling is observed and the increase of data quality is somehow almost linear for the range from 1 to 9 replicates, percentages between 60 – 80% for sub-groups with 6 – 9 replicates (for 50 and 100 initial molecules) seem to show a possibly reasonable number of replicates for real-time PCR assays in 200 nl. Using the

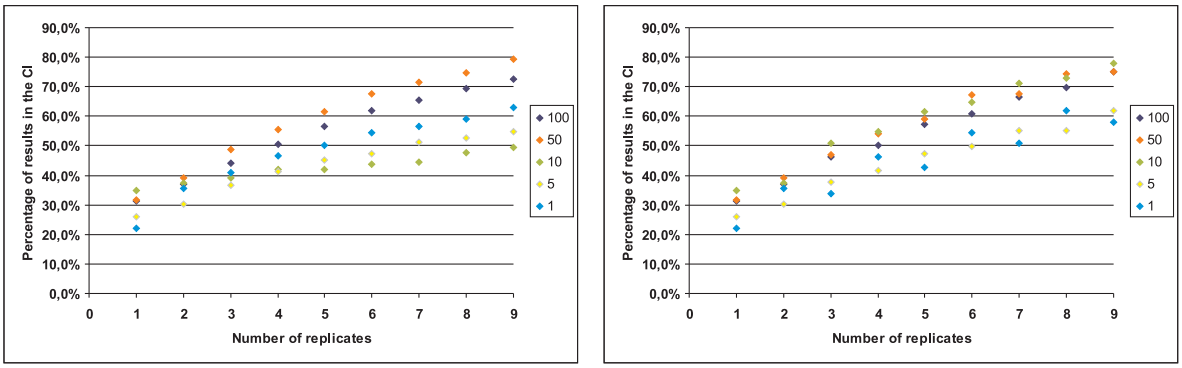

(a) Mean based **(b)** Median based

Figure 30: The percentage of mean (**a**) and median (**b**) from subsamples of different size (number of replicates), which lays in the confidence interval of the original data set (N=60) is plotted. This has been done for 5 different initial target concentrations (see legend for molecule numbers). Template was hgDNA, performed were RNAse P standard TaqMan assays in 200 nl.

median calculation seems to be an option in case of outliers.

3.5.4 The dynamic range of 200 nl TaqMan assays

To evaluate the dynamic range of the µPCR chip platform, 200 nl RNAse P TaqMan assays were performed spanning a large range of target concentrations. As template a small PCR fragment (2.9.1) covering the target sequence of the RNAse P Taqman assay was used to allow high numbers of initial target molecules. This was not possible with hgDNA, since high concentrations showed dispensing problems caused by sticking effects at the nozzle tips. Initial numbers of target molecules per reaction were 40, 4×10^3, 4×10^4 and 4×10^5, 21 replicates each. The obtained Ct-values were 28.7±0.69, 21.1±0.35, 18.3±0.40 and 15.2±0.74, respectively. This resulted in CVs from 1.7% to 4.9% and respectively 27% – 65% deviation in initial target molecules, both comparable to the variation found in the concentration gradient experiment performed on hgDNA (see 3.5.2). The resulting standard curve had a correlation coefficient of 0.9946, and the assay efficiency was 96.7%, furthermore supporting the assumption that adhesion effects of DNA molecules in dispensing devices are correlated to the complexity of the molecules. Moreover it suggests that the herein developed system is suitable for real-time PCR over a range of at least 4 orders of magnitude in 200 nl reactions.

3.5.5 Chip-to-chip reproducibility

For investigation of inter-experiment variation (inter-chip variation) with our platform, two µPCR chips were identically preloaded with cDNA from three mouse tissues (brain, liver, kidney). After filling with reaction mix the chips were identically processed to

quantify the transcript levels for 5 genes (see 2.2.3). Resulting Ct-values for both chips were plotted against each other (Figure 31). The linear regression shows a slope of

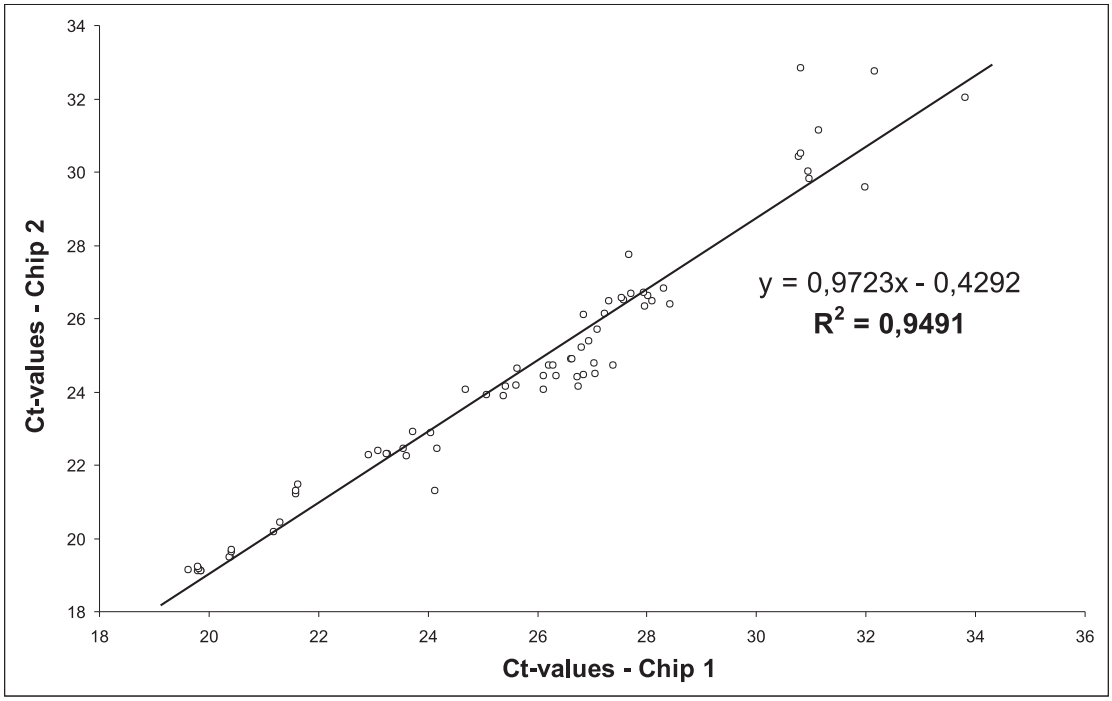

Figure 31: Linear regression analysis for Ct-values of two identically performed experiments in the 1k-format µPCR chip to demonstrate the chip-to-chip reproducibility of the system.

0.97 and a correlation coefficient of 0.95 indicating a good reproducibility between both experiments. Some variation was denoted especially for Ct-values above 30 cycles, where the initial amount of template is low. Comparing absolute Ct-values of both chips or just taking a point at the regression graph and comparing x and y values show an offset of approximately one between both µPCR chips. This can be caused by differentially set analysis parameters like the manual setting of the threshold. Reproducibility is given, if the results on both chips are consistent to each other, which is shown by a good correlation. The correlation coefficient close to one is the measure of reproducibility between both chips. There are few spots that lay quite far away from the regression line. Especially above a Ct-value of 30 the inter-chip variation is slightly increased. Outliers can be caused by the concurrence of two extreme diverging events. These events can be due to single irregularities mainly in the dispensing or due to the impact of systematic noise, which has a differing frequency for both chips. The increased variation above 30 cycles shows the general systematic effect of high Ct-values on variation and reproducibility, which is already known from large volumes.[62]

3.6 Further reduction of assay volume

3.6.1 Volume reduction using the 1k/V-µPCR chip

Appearing optical distortion at volumes below 200 nl limits the minimal working volume for the 1k-format of the µPCR chip to 200 nl. The 1k/V-format of the µPCR chip enables a further reduction of the assay volume due to its V-shape of the individual reaction vessels (see 2.4.2). In a concentration gradient experiment wells were preloaded with 100 nl of four concentrations RNAse P TaqMan flanking PCR product using the Sciclone valve dispenser with oil separation. Resulting numbers of initial target molecules were 1.1×10^5, 1.1×10^4, 1.1×10^3 and 1.1×10^1 per well. PCRs were performed with a final reaction volume of 100 nl and 50 nl.

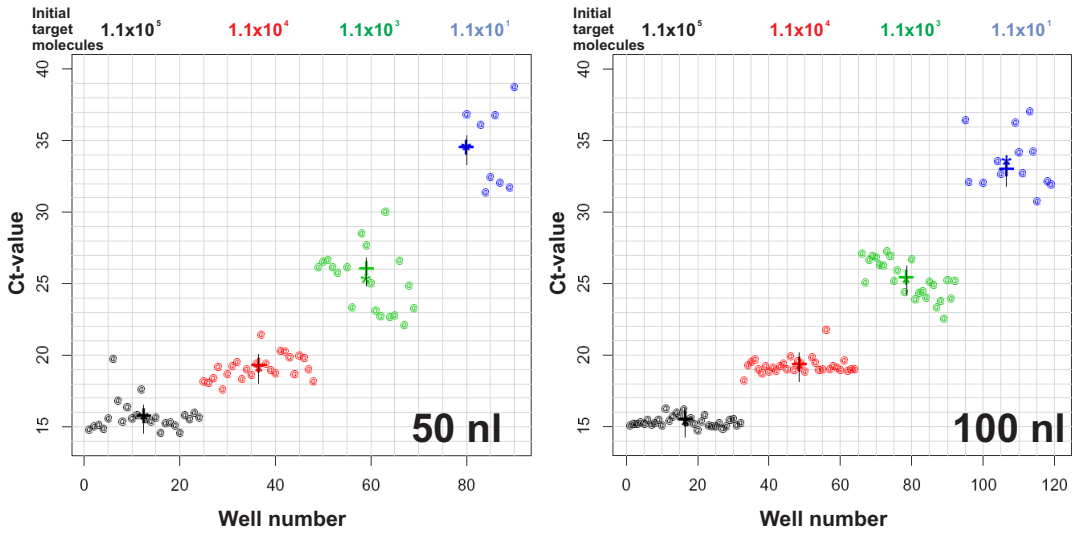

(a) Ct-values for all 100 nl assays **(b)** Ct-values for all 50 nl assays

Figure 32: Further reduction of real-time PCR assay volumes with the 1k/V-format of the µPCR chip. **a)** A plot of all Ct-values for 100 nl TaqMan Rnase P assays on 4 different target concentrations. **b)** Ct-values of the 50 nl assays. Variation is slightly higher than for the 100 nl assays.

Figure 32 shows plots of all Ct-values for each volume. In both volumes the variation of Ct-values is increased with decreasing numbers of initial target molecules, represented by the respective standard deviations (Table 14), and concordant to the results for the 200 nl volumes. This is particularly apparent in the data of the 50 nl experiment, and can be partially explained by the higher sample pre-loading volume of 100 nl. Despite centrifugation during drying, sticking target molecules on well parts above the 50 nl filling level are possible, which influences the target concentration in the PCR reaction. Increased variation is also shown by more failing reactions in the low target molecule range; the number of failing reaction correlates to the lowering of initial target molecules.

Table 14: Results from 100 nl / 50 nl RNAse P TaqMan assays. $PCR_{performed}$ – total number of performed reactions, $PCR_{failures}$ – percentage of failing amplifications without detectable PCR product, R_2 Pearson Correlation Coefficient of standard curve (not plotted).

Initial molecules	**Ct-value**	**$PCR_{performed}$**	**$PCR_{failures}$**
100 nl reactions			
1.08E+05	16.5±0.6	32	0.00%
1.08E+04	21.1±0.7	32	3.13%
1.08E+03	27.1±1.2	28	10.71%
1.08E+01	35.4±2.6	28	57.1%
$R_2 = 0.995$			
PCR-Efficiency= 61.7%			
50 nl reactions			
1.08E+05	17.0±1.6	24	0.0%
1.08E+04	20.8±1.0	24	0.0%
1.08E+03	28.0±4.2	21	9.8%
1.08E+01	35.6±2.5	21	66.7%
$R_2 = 0.983$			
PCR-Efficiency= 60.8%			

3.6.2 Volume reduction using the 4k-µPCR chip

The further reduction of assay volumes was not possible with the 1k-format µPCR chips. Optical irritations and inefficient excitation do not allow reaction volumes below 50 nl. A next step down to a volume below 20 nl was done with the 4k-format of the µPCR chip, following the standard workflow (3.3). Due to the low volume the piezo dispenser was used to preload the chip with hgDNA in a gradient of 3 quantities: 8, 16 and 24 molecules per well. Samples were dried down. Afterwards the mix for the RNAse P TaqMan assay was dispensed using the piezo dispenser as well. The chip was processed in the real-time detection unit under standard conditions as described for the 1k-format.

Generated real-time plots (Figure 33 b + c) show a noisy course of fluorescence intensity. This is caused by imbalances in the power supply, which directly effects the excitation intensity. Variation of results seem to be particularly increased for assays with 8 initial target molecules. Figure 34 shows mean and median Ct-values for the different target concentrations, of rowwise arranged clusters on the chip. Outliers were removed using the standard procedure. Mean and median were taken to see, whether the values follow a normal distribution, which seems to be given.

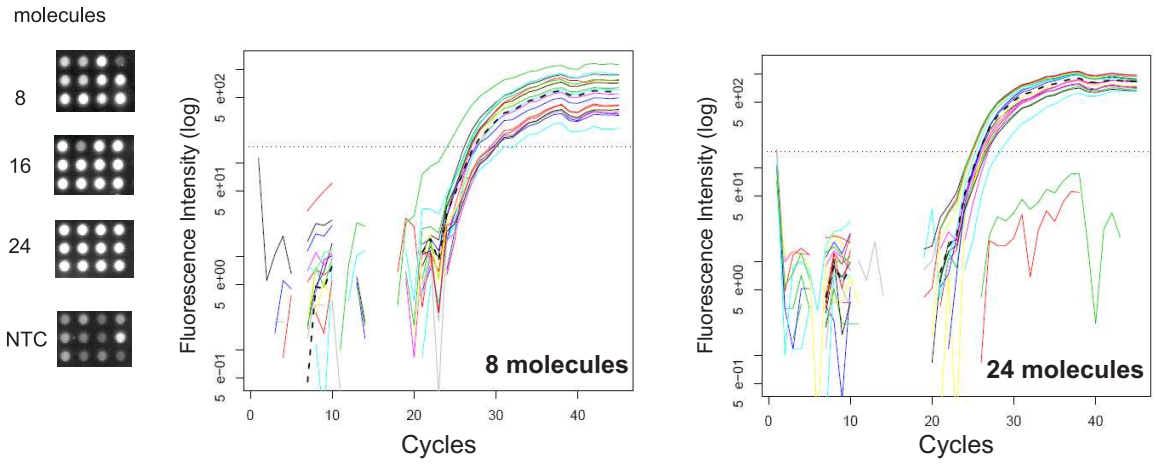

(a) 4kChip

(b) real-time plot with initial 8 target molecules

(c) real-time plot with initial 24 target molecules

Figure 33: a) Selected wells from the 4k-chip at end point. **b)** Real-time plot for a RNAse P Taqman assay with initially 8 target molecules (hgDNA). **c)** Real-time plot for the same assay with 24 initial target molecules.

Despite a difference in target molecules, no difference in Ct-values between assays with 16 and 24 initial molecules can be seen. Only assays of the lowest target concentration (8 molecules per well) show a difference of approx. 2 cycles to the next concentration, which corresponds to a 4-fold change in target concentration instead of the expected 2-fold change. In general Ct-values do not clearly correlated with the

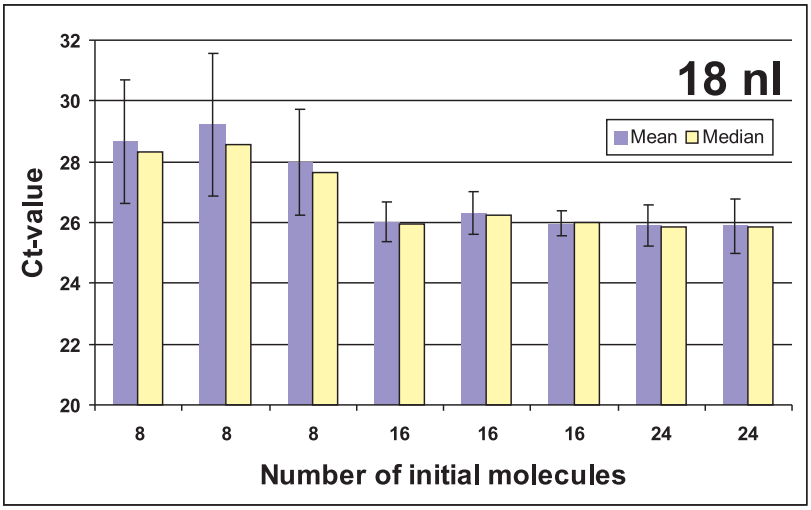

Figure 34: 18 nl RNAse P TaqMan assays on three different quantities of hgDNA: 8, 16 and 24 molecules per well. The arithmetic mean and median were computed, to compare an outlier sensitive measure with an outlier non-sensitive measure.

initial target concentrations. Reason for this might be the mixing between sample and system fluid in the dispenser nozzle during sample as well as mix distribution. Due to the promising results in 200 nl, this volume and the 1k-µPCR chip was finally chosen to study tissue specific expression in mouse.

3.7 Application: Miniaturized real-time PCR based expression profiling in mouse

In order to validate the µPCR chip platform as a tool for real-time PCR a small-scale gene expression study was performed in three mouse tissues (brain, liver and kidney). Transcript levels of five genes were investigated in parallel using the µPCR chip platform with 200 nl reaction volumes, and for comparison of a standard real-time PCR with 10 µl reaction volumes. All reactions were performed with identical standard TaqMan assay concentrations (2.2.3), using the same concentration of total RNA, which corresponds to a total amount of 12.5 ng for 10 µassays and 0.25 ng for assays in 200 nl. The replicate number was 6 and 4 for the 200 nl assay and the 10 µl assay respectively. Figure 35a

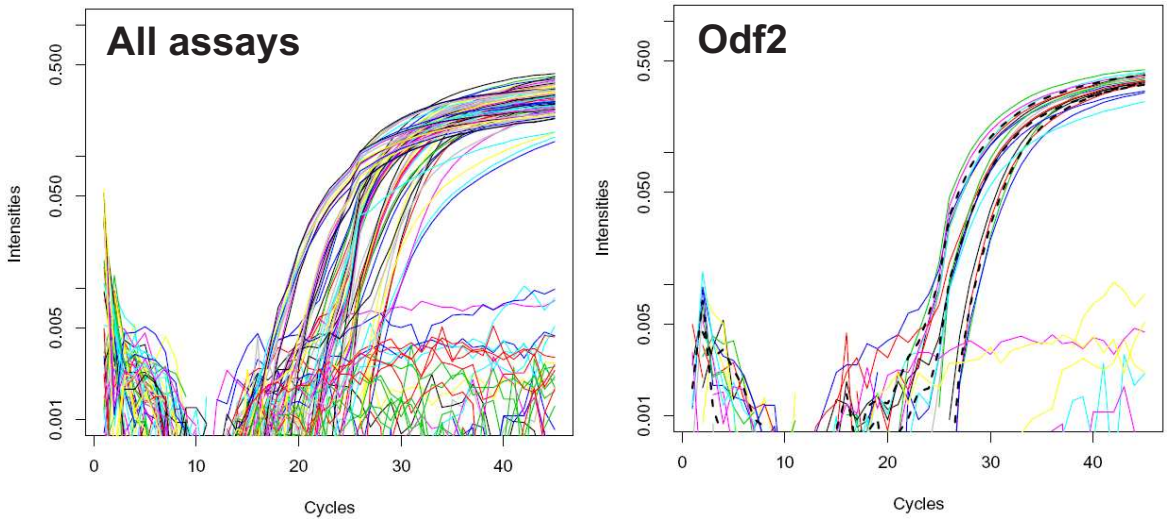

(a) Amplification plot of all genes and tissues in 200 nl

(b) Amplification plot for gene *Odf2* in 200 nl

Figure 35: Amplification plot of mouse expression analysis in the µPCR chip. **a)** Amplification plot for 200 nl real-time PCR of all genes in all tissues, brain, liver and kidney. **b)** Selected amplification plot of the gene *Odf2*. The dotted lines are averaged lines for each tissue, respectively.

shows the amplification plots obtained for all 200 nl assays and Figure 35b illustrates the tissue specific amplification plots for the gene *Odf2*. A detailed presentation of all data can be found in the appendix Table 16. A comparison of averaged absolute Ct-values is depicted in Figure 36a and 36b for brain and kidney. The results obtained from the 200 nl experiment are obviously comparable to the standard real time PCR experiment. Differences appear in the variation of results, that is greater in 200 nl experiments, with standard deviations ranging mainly from 0.05 to 0.90 Ct. Whereas in the standard assays, standard deviations ranged from 0.02 to 0.18. Only for the very low expressed *Cacna1g* gene in kidney, an exceptional high standard deviation of 1.49 Ct for 200 nl assays and 0.31 Ct for 10 µl assays was observed. Ct-values seen (Figure 36a and 36b) for the 200 nl assays tend to be proportionally higher than in 10 µl;

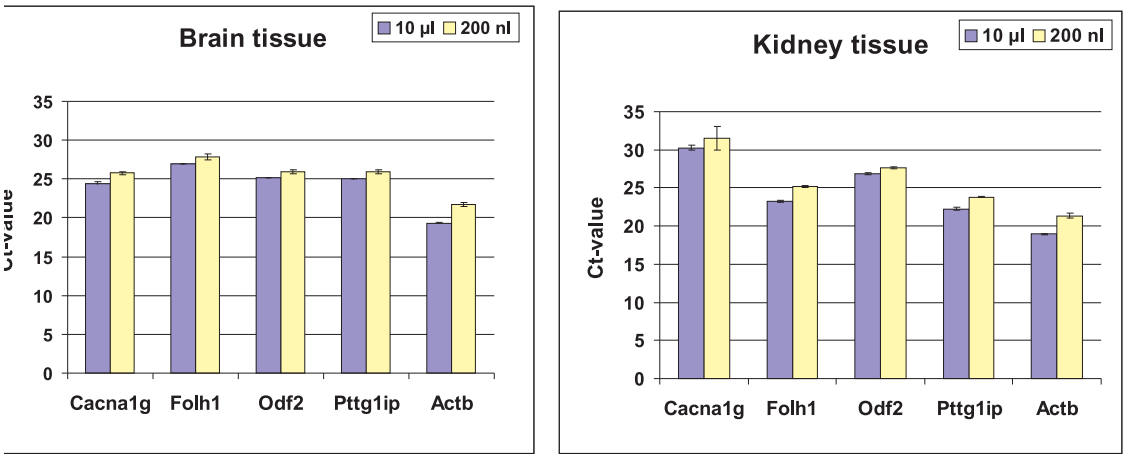

(a) Ct-values for brain tissue

(b) Ct-values for kidney tissue

Figure 36: Comparison of absolute Ct-values for two tissues in mouse expression analysis. Histograms show the Mean Ct-values with their standard deviations obtained for brain **(a)** and kidney **(b)** tissue in 10 l and 200 nl volumes. The 10 µl and 200 nl reactions were done with 4 and 6 replicates, respectively.

this is caused by the manual threshold settings, but does not affect the quantification results, as shown below. For relative quantification the $\Delta\Delta$Ct method[103] was used for both experiments (2.10.5). Each gene was normalized to betaactin (*Actb*) and the fold change of the gene's expression relative to kidney was calculated. In Figure 37 the results obtained for brain are shown. Genes under represented in kidney compared to brain show values below, over-expressed above zero. *Cacnag1*, a calcium channel subunit, was found 70 times (68× in 200 nl; 72× in 10 µl) more expressed in brain than in kidney, whereas it could not be detected in liver in both experiments. *Folh1*, outer dense fiber gene of sperm tails, was 0.2 or 0.1 times less expressed in brain than in kidney in 200 nl and 10 µl experiments respectively, and it was not detected in liver. *Odf2* was over expressed by a factor 4 (4.2 in 200 nl and 4.3 in 10 µl) in brain relative to kidney and the level of expression in liver was comparable to kidney with fold-changes of 4.4 (10 µl) and 3.8 (200 nl). Finally *Pttg1ip*, the pituitary tumor-transforming 1 interacting protein, is under expressed in brain with a brain/kidney fold change of 0.3 in 200 nl reactions and 0.2 in 10 µl volumes. In liver *Pttg1ip* showed a similar expression pattern with fold changes of 0.1 and 0.1 in nano and standard volumes respectively. In conclusion, *Cacna1g* and *Odf2* are clearly more strongly expressed in brain whereas *Folh1* and *Pttg1ip* have the highest expression in kidney and liver, respectively.

This validation study clearly shows concordance in gene-expression results between 200 nl and 10 µl. Results obtained in 10 µl assays confirmed the results from the µPCR chip platform using 200 nl TaqMan assays.

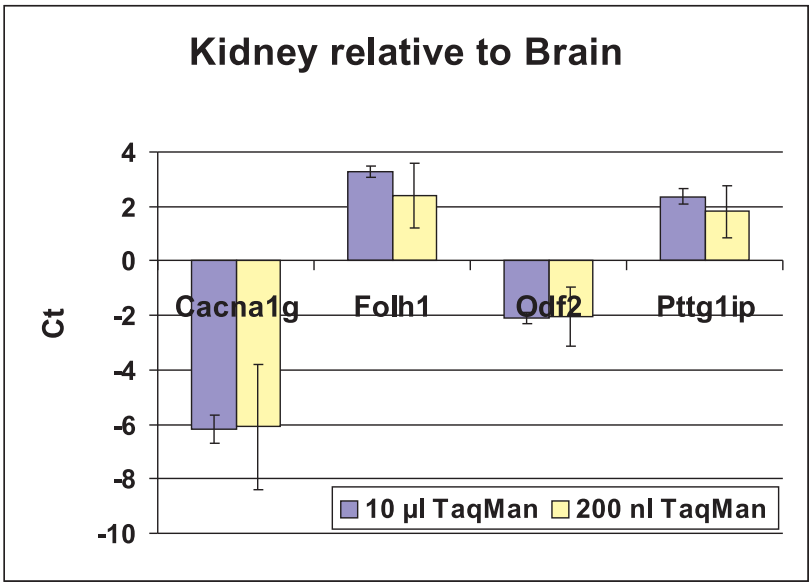

Figure 37: Relative quantification in 200 nl. Relative quantification was performed using the $\Delta\Delta$ Ct method[103] for both experiments. Each of the genes was normalized to *Actb* and the change in normalized Ct-values from kidney relative to the brain sample was calculated. Genes under represented in kidney compared to brain show values below 0, over-expressed above 0.

3.8 Application: TaqMan based genotyping in nanoliter assay volumes

As a second application beside real-time PCR, TaqMan based SNP genotyping was performed on the µPCR chip platform. For endpoint read-out of signal intensities of at least two dyes a detection unit was built up (see 2.8.1). Excitation and emission filters for the dyes VIC and FAM were chosen according to their spectra, and an allele calling algorithm was developed.

3.8.1 Algorithm for allele calling of 200 nl genotyping assays

Due to their excellent clustering and allele calling under standard conditions in 10 µl volumes (see appendix Figure 47), the assays SNP IGR2198a and 2230 were chosen for a first test in 200 nl volumes. 200 nl assays were conducted following the standard workflow (3.3) and standard concentrations for SNP genotyping (2.2.4). Each well was preloaded with 1 ng hgDNA, which equals approx. 300 molecules. After performing the assays, fluorescence measurements for several filter combinations were done with the custom made SNP genotyping detection unit (2.8.1). For allele calling the following fluorescence measurements were used: the $\mathrm{FAM}_{Excitation}/FAM_{Emission}$ (FAM) filter combination, $\mathrm{FAM}_{Excitation}/VIC_{Emission}$ (FAMVIC) filter combination and the $\mathrm{VIC}_{Excitation}/VIC_{Emission}$ (VIC) filter combination. A background signal from an empty plate was taken from the FAM filter combination (FAM_BG). Calculation of a

SNP discrimination index after the following equation lead to the best discrimination results:

$$INDEX_{SNPDiscrimination} = FAMVIC - 2 \times FAM + FAM\_BG \tag{9}$$

Values were calculated and visualized with self developed scripts (see A.4.2) using the R statistics environment. Clusters of genotypes were manually determined by setting of thresholds (see Figure 38 d).

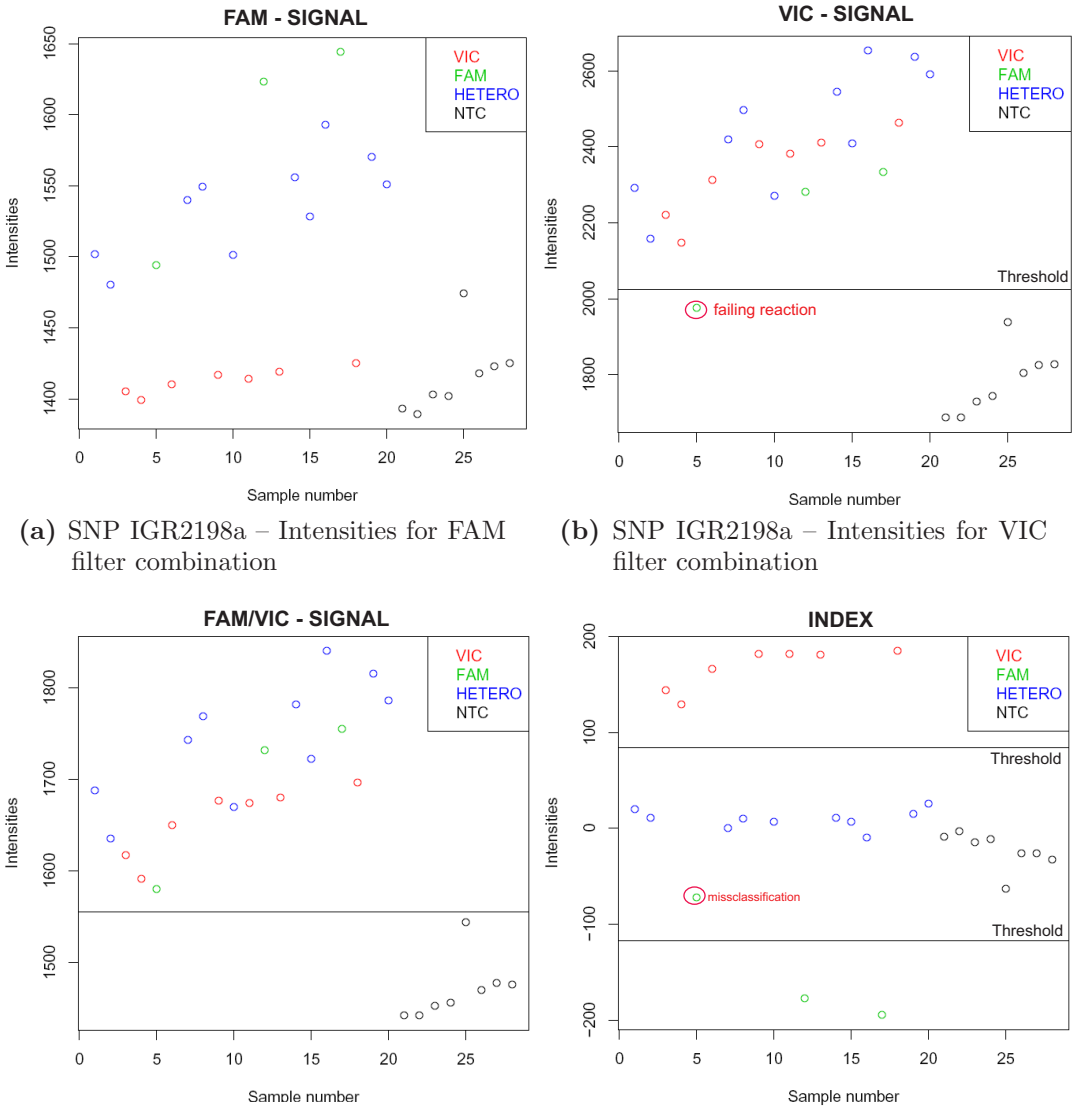

(a) SNP IGR2198a – Intensities for FAM filter combination

(b) SNP IGR2198a – Intensities for VIC filter combination

(c) SNP IGR2198a – Intensities for FAM/VIC filter combination

(d) SNP IGR2198a – Intensities for calculated INDEX

Figure 38: Shown are fluorescence intensities for accurate performing 200 nl TaqMan genotyping assay SNP IGR2198a with different filter combinations. **a)** Absolute intensities of FAM filter combination, **b)** absolute intensities of the VIC filter combination. The threshold is set to separate positive reactions and non-template controls. **c)** shows the FAMVIC signal intensity and **d)** the resulting INDEX value, clustering in three intensity ranges for three genotypes.

Intensities of the FAM filter combination (Figure 38 a) allow to clearly discriminate homozygous FAM and heterozygous samples from the homozygous VIC samples. The FAMVIC filter combination allows to discriminate the heterozygous samples, which show here the highest intensity. This results in the highest INDEX values for VIC homozygotes. FAM homozygotes comprise the lowest values and heterozygotes range between FAM and VIC homozygotes.

As shown in Figure 38 d non-template controls are found to be classified as heterozygous samples. To avoid misclassifications due to failing PCRs, the VIC intensity was taken as reference for failing reactions. Samples with a VIC intensity near to and below the intensity of the non-template controls were regarded as failing reactions and therefore rejected. In the shown assay one miss-classification appeared (Figure 38 d). This might have been due to a suboptimal performing reaction, since the VIC signal intensity of this assay is rather low and close to the values for the non-template controls (Figure 38 b). This is shown in the 200 nl results of the SNP IGR2198a (Figure 47 c).

For the second SNP 2230 the data are not consistent to the results from the large volumes. Although the assays performed well in 10 µl (see appendix 47), no definite allele calling was possible in 200 nl (Figure 39 b). This is caused by a suboptimal

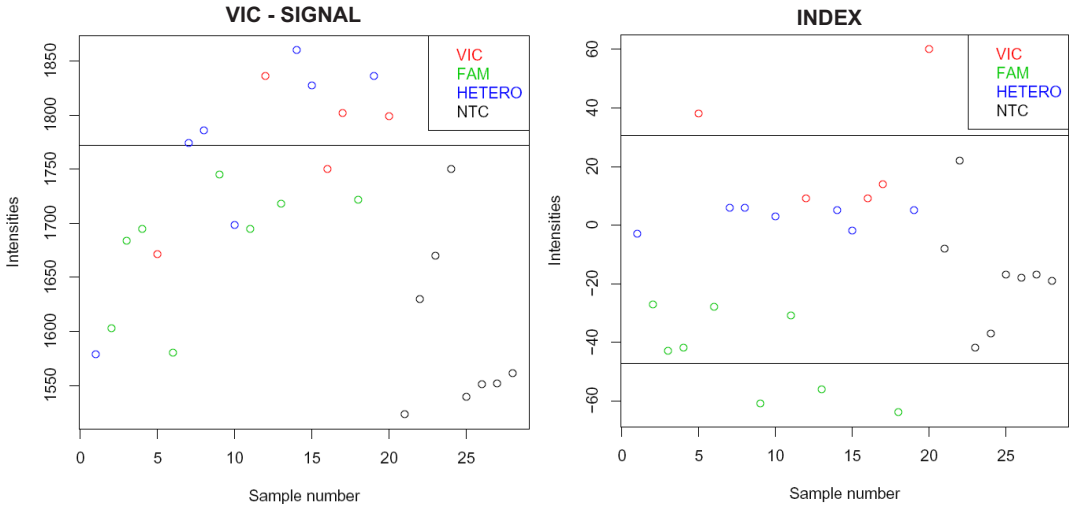

(a) SNP 2230 – Intensities for VIC filter combination

(b) SNP 2230 – Intensities for calculated INDEX

Figure 39: Fluorescence measurements for badly performing 200 nl TaqMan SNP genotyping assay SNP 2230. **a)** VIC intensities show no separation of NTCs. **b)** Intensities of the caclulated INDEX without any clustering of genotypes.

performing assay, which becomes obviously in the VIC fluorescence data (Figure 39 a). Overlaps between VIC intensities of non-template controls and samples indicate a poor performance.

Enzyme concentration

A good PCR performance seem to have direct impact on the genotype discrimination. Thus 200 nl assays were performed with increased enzyme concentrations of additional 0.025 U per 200 nl reaction Taq polymerase (Amplitaq Gold, Applied Biosystems). This led to an improved allele calling for the well performing SNP IGR2198a assay. For the suboptimal performing SNP 2230 assay no improvements in clustering were observed (Figure 40). Thus it is concluded, that the clustering can be improved by increasing

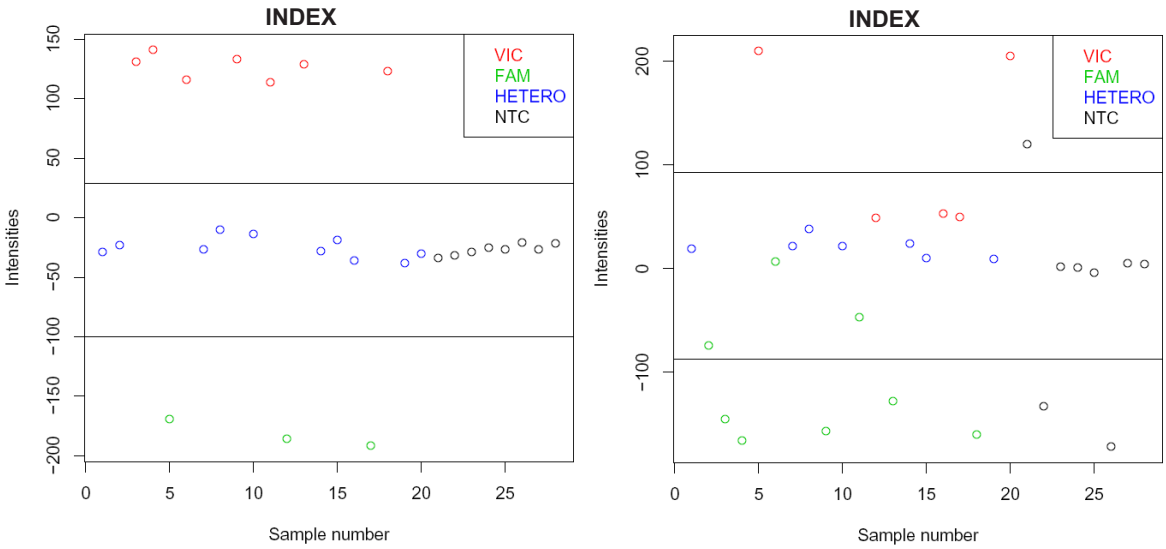

(a) Allele Calling for SNP IGR2198a in 200 nl with increased enzyme concentration

(b) Allele Calling for SNP 2230 in 200 nl with increased enzyme concentration

Figure 40: Impact of enzyme concentration on allele calling in 200nl assays, using the conventional TaqMan reaction mix. **a)** Improved clustering for the SNP IGR2198a assay. **d)** No improved clustering for the SNP 2230 assay, the assay quality seem to be more important.

the enzyme concentration, but in general the assay quality seems to have the strongest impact on data quality. In 200 nl poor performing assays like the IGR2198a assay can not be improved by increased enzyme concentrations.

3.8.2 Verification of the allele calling algorithm

To evaluate the allele calling algorithm developed (Equation 9), SNP genotyping was performed in 200 nl for 20 patient samples and 10 SNP's. Samples were dispensed with individual nozzles for each patient to avoid cross contamination. The reaction mix was distributed on clusters of 4×8 wells (20 samples & 12 non-template controls) using one nozzle to minimize volume differences in the final reaction volume. Each assay was performed on three independent clusters, except two assays, which could only be performed in two clusters due to limited space on the chip. Three from 10 assays (rs2631367, 2011 and 2230) performed insufficiently. One assay (05GR2096a) completely failed in the third replicate, which was caused by an error during mix distribution. Failing reactions were randomly distributed. Only one patient sample showed an accumulation of failing

/ misclassified reactions in almost all clusters. This could be caused by problems during the DNA dispensing with the respective nozzle or by a bad DNA quality. Excluding the failing assays and the problematic sample, the fraction of failing reactions is ≤ 1 reaction per 20 assays. Only the first cluster of the SNP X100 differs from this. A comprehensive summary of results can be found in the appendix Table 19.

3.8.3 Limiting target concentrations for SNP genotyping in 200 nl

Beside DNA quality the genotyping quality is influenced by the amount of available target molecules. To identify a limiting DNA concentration for valid TaqMan based SNP genotyping in 200 nl, a study with several DNA concentrations was performed. µPCR chips were preloaded with 150 nl hgDNA or WGA-DNA samples from 4 patients (center codes: 36748, 36746, 36790, 36761) representing all genotypes ($1 \times HOMO$ 1, $1 \times HOMO$ 2, $2 \times HETERO$) for the SNPs 2063 and IGR2198a. Highest concentration was concentration 1 with 5 ng/µl, equivalent to a final number of 225 molecules hgDNA per well. Further concentrations 2 – 8 were successive dilutions leading accordingly to 150, 75, 53, 38, 19, 9 and 5 molecules hgDNA or the equivalent amount of WGA-DNA per well. The quality of allele calling was investigated by evaluation of clustering. Ideally three clusters representing the three possible genotypes should be seen. In Figure 41 a an optimal clustering is shown. In contrast, no clear identification of three

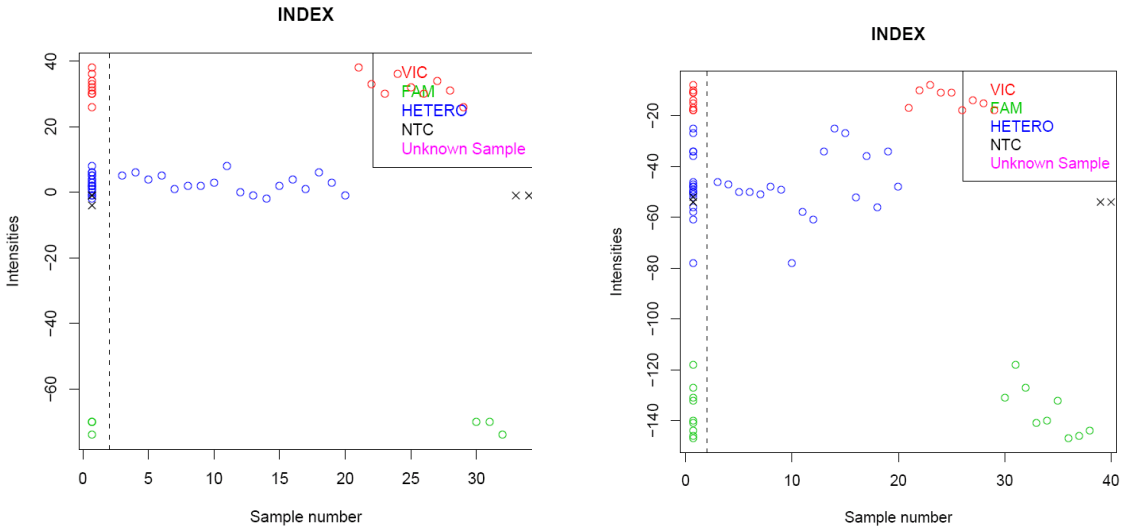

(a) Perfect clustering **(b)** No clear clustering

Figure 41: Graphical output from R using the allele calling algorithm. The left 'column' of points is a accumulation of all INDEX intensities on one x-axis position to check for three genotype clusters in y-axis orientation. The top cluster is the VIC homozygotes cluster, the bottom cluster is the one of the FAM homozygotes and heterozygotes cluster between them. On the right hand side of each plot all INDEX values of one SNP assay are plotted again, but with changing x-axis positions to identify INDEX values of individual wells. Expected genotypes are color coded as shown in the legend. **a)** Good clustering of all three genotypes which allows perfect allele calling. **b)** No clear clustering caused by spreading INDEX values for the second half of the heterozygous samples.

clusters is possible in Figure 41 b, demonstrating suboptimal clustering. This is caused by mixing INDEX values of VIC homozygotes and heterozygotes.

After sample pre-loading first genotyping was performed under standard conditions for the SNP 2063 using the standard TaqMan® reaction mix. The results for hgDNA as well as WGA-DNA are summarized in Figure 42. Assays with genomic

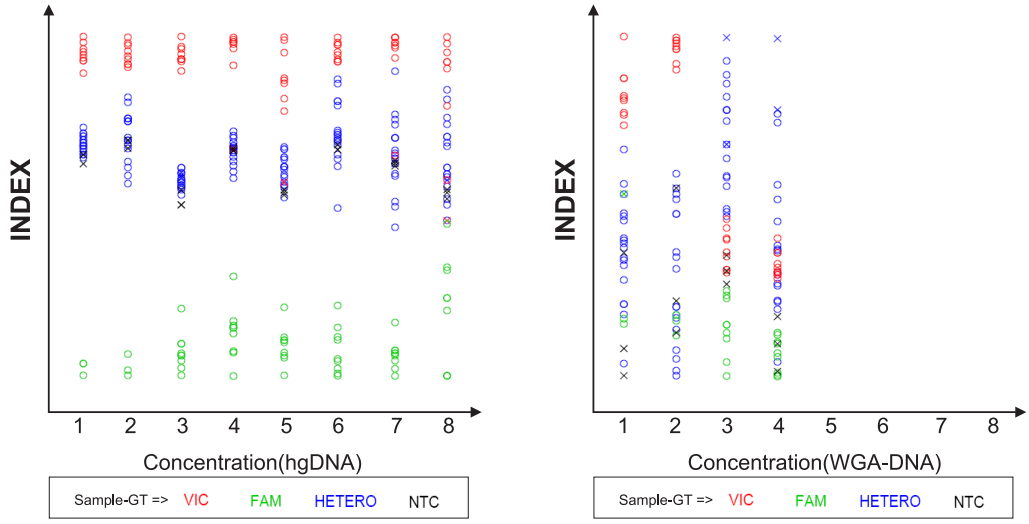

(a) SNP 2063 on hgDNA **(b)** SNP 2063 on WGA-DNA

Figure 42: Clustering quality for SNP 2063 with conventional TaqMan reaction mix in 200 nl volumes. Failing reactions are marked as '×', the expected genotypes are color coded like in the legend.

DNA samples show a good clustering down to concentration 4 (53 molecules). Below this concentration no distinct clustering of INDEX values is obtained. WGA-DNA samples show no clear clustering for all concentrations. Whole genome amplification of DNA is a widely used step in SNP genotyping studies to enlarge the amount of available (and precious) sample.

Since usual template concentrations were used and no problems of sensitivity are known from the real-time expression studies, it was tried to improve the clustering for WGA-DNA samples by using a newly developed GT TaqMan® reaction mix from ABI, which has been especially designed for genotyping. The results of an identically performed experiment to Figure 42, except the new GT reaction mix, are shown in Figure 43.

Surprisingly not only for the WGA-DNA samples, but also for the genomic DNA samples, the cluster quality could be significantly improved. The hgDNA as well as the WGA-DNA samples show good clustering down to the 7^{th} concentration. The 8^{th} concentration shows spreading INDEX values especially for heterozygotes. This could be caused by differing distribution of both alleles during dispensing, since only 5 target molecules are theoretically in one well, which means 2.5 molecules per allele. To verify this result for the new GT TaqMan reaction mix the same experiment should

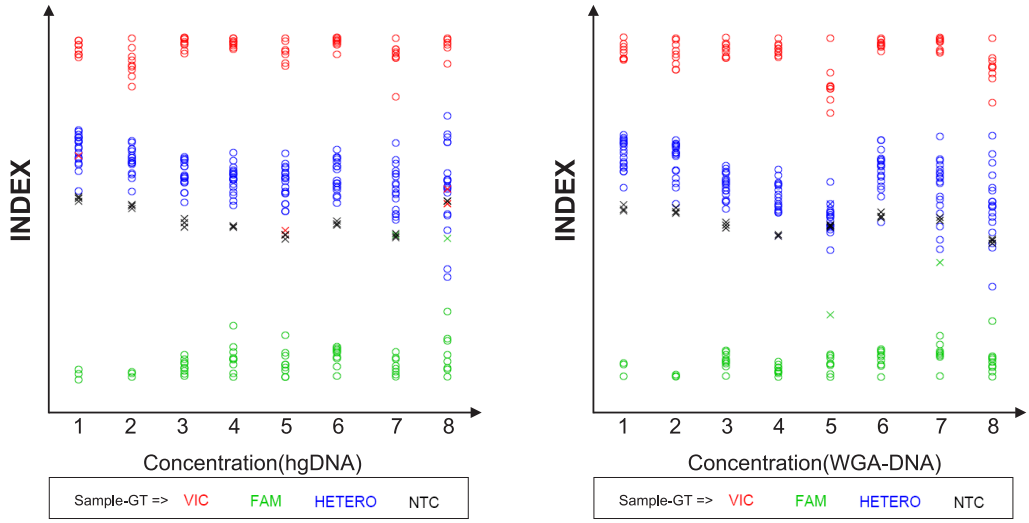

(a) SNP 2063 on hgDNA **(b)** SNP 2063 on WGA-DNA

Figure 43: Clustering quality for SNP 2063 with new GT reaction mix in 200 nl volumes. Failing reactions are marked as '×', the expected genotypes are color coded like in the legend.

be repeated with other genotyping assays. The results for SNP IGR2198a (Figure 44) confirm the previous findings.

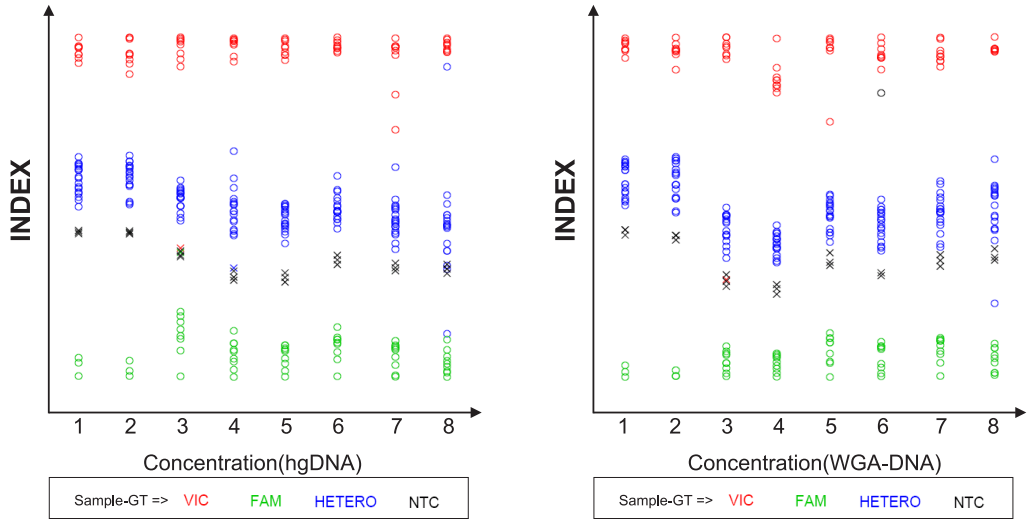

(a) SNP IGR2198a on hgDNA **(b)** SNP IGR2198a on WGA-DNA

Figure 44: Clustering quality for SNP IGR2198a with new GT TaqMan reaction mix in 200 nl volumes. Failing reactions are marked as '×', the expected genotypes are color coded like in the legend.

3.8.4 Further volume reduction – SNP genotyping in 100 nl

Miniaturization of reaction chambers and volumes inherently leads to the reduction of initial target molecules, which contributes to the increased variation. To investigate the effect of a further volume reduction and limiting target concentrations, a 1k/V-format of the µPCR chip was preloaded with the same total amount of DNA as shown above. TaqMan SNP genotyping was performed in 100 nl for the SNP IGR2198a using the new GT reaction mix. The results in Figure 45 show a comparable clustering quality to the 200 nl experiment for the same assay. Only the WGA-DNA sample

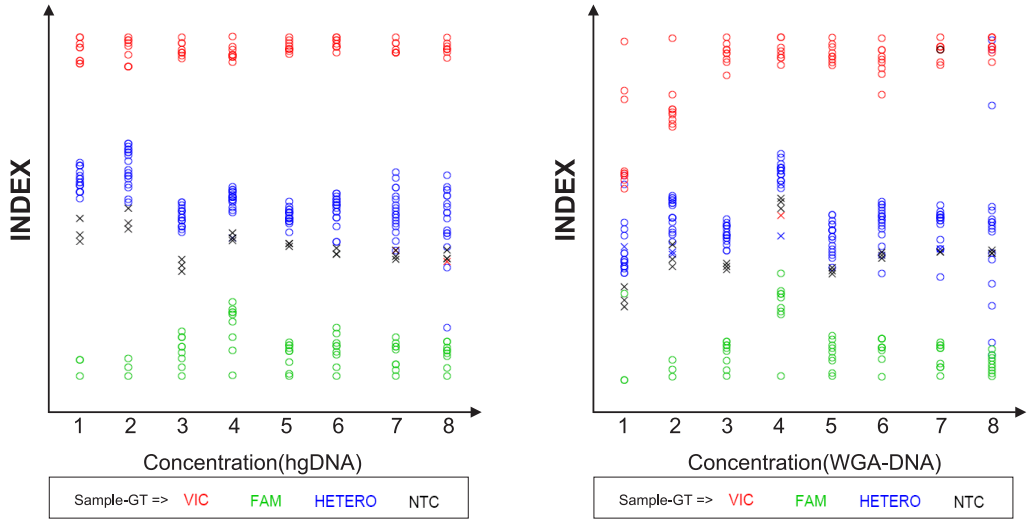

(a) SNP IGR2198a on hgDNA **(b)** SNP IGR2198a on WGA-DNA

Figure 45: Clustering quality for SNP IGR2198a with new GT reaction mix in 100 nl volumes. Failing reactions are marked as '×', the expected genotypes are color coded like in the legend.

concentrations 1 and 4 show no ideal clustering. For concentration 4 this is more likely caused by abnormalities in the mix dispensing, than a sample concentration effect, since the neighboring concentrations show good clustering. For the highest concentration it might be a concentration effect.

To improve the signal intensity of the endpoint measurement, processed chips were turned upside down and shortly centrifuged before signal read-out. Appearing optical distortions below assay volumes of 100 nl were limiting for further volume reduction.

3.8.5 Validation study for 200 nl genotyping

For validation of the platform a 200 nl SNP genotyping study with full coverage of the µPCR chip was performed. According to the standard workflow 150 nl aliquotes of 60 patient samples were preloaded to the chip, arranged in 16 clusters each for another SNP. Genomic DNA samples were used in a concentration of 5 ng/µl. For optimal performance the new GT TaqMan reaction mix was used. Other assay components were kept like described above (see 2.2.4). After performing the assays genotypes were determined with the developed algorithm. The retrieved genotypes were compared to the data from the cooperation partner in Kiel, which are shown in Figure 46 and comprehensively shown in Table 20. Concordance rates are calculated on basis of all

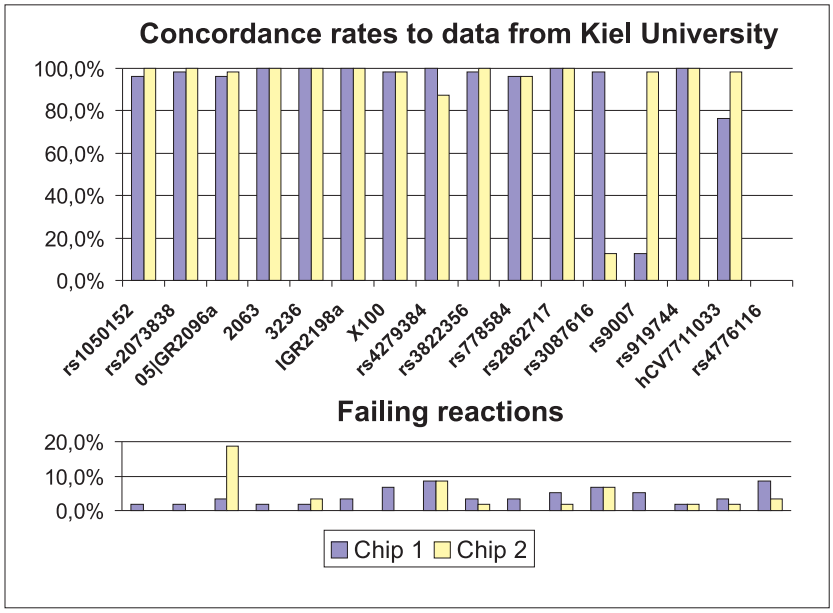

Figure 46: Rates of concordance to the data from Kiel for the first and second chip. Shown is the concordance* rate, which was introduced due to an accumulation of wrong allele calling for 4 samples in all targets. This is presumably caused by a DNA dispensing problem during the sample preloading or bad DNA quality, and does not reflect the assay performance itself. The comprehensive data set can be found in Table 20.

reactions reduced by the number of failing reactions. To calculate the concordance* rate 4 samples were removed from the data set, because they showed concordance of only 41.8% across all targets. This second concordance rate was introduced to remove obvious sample dispensing caused effects from the data set. The average failing rate for Chip 1 and Chip 2 was 3.8% and 2.9%, respectively, which approximately corresponds to in average 2 failing reactions per 60 assays. On both chips one SNP cluster showed no clear clustering resulting in misclassification near 90%; for SNP rs9007 on chip 1 and SNP rs3087616 on chip 2. Removing these both clusters from further analysis results in average concordance rates for Chip 1 and 2 of 93.9% and 94.7%, respectively. The impact of the 4 suspect samples becomes apparent with average concordance* rates of 97.0% and 98.3% for chip 1 and 2, respectively.

For the SNP rs4776116 no data from large volumes is available. The obtained INDEX values show no clear clustering in three point clouds. Referencing the SNP database at the National Center for Biotechnology Information(NCBI) the minor allele (allele G/FAM) has a frequency of 3.7%. For 60 patients I would expect 2 G or FAM homozygotes. Due to the high probability of a total missing of the second homozygous genotype I conclude, that in the sample of 60 patients only homozygotes C and heterozygotes a present. This is supported by the fact, that samples with lower INDEX values cluster together with the NTCs, which is typical for heterozygous samples. Comparing the chips with each other, both show full accordance of genotypes except for failing reactions.